وزارة التعليم العـــالي والبحث العلـمي
جامـــعة بابـــل
كليـــة التربية للعلوم الصرفة
قســـم الفيزيـــاء
الدرسات العليا (الماجستير)

دراسة التركيب النووي لبعض النوى المختارة بالقرب من النواة ^{56}Ni باستخدام تفاعل سكيرم هارتري–فوك

رسالة مقدمة
إلى مجلس كلية التربية للعلوم الصرفة في جامعة بابل
وهي جزء من متطلبات نيل درجة الماجستير
في التربية / الفيزياء

من قبل

نورس طالب شهاب احمد

بكالوريوس تربية فيزياء
جامعة بابل (2002)

بأشراف

أ.د.فؤاد عطية مجيد
كلية التربية للعلوم الصرفة
قسم الفيزياء

1444 هـ **2022 م**

الخلاصة

اصبح العثور على توزيعات الشحنة وكثافة الانتقال للنواة ممكنا عن طريق الاستطارة الالكترونية . ستتمكن النوى قصيرة العمر الغنية بالنيوترونات قريبا من الوصول الى هذه الاداة .

في هذه الدراسة تم التحري عن عوامل التشكل للاستطارة الالكترونية المرنة $|F_{C0}(q)|^2$ وتوزيع كثافة الشحنة (CDD) للحالة الارضية 0^+ للنيكل ^{58}Ni والزنك ^{64}Zn والجرمانيوم ^{70}Ge والجرمانيوم ^{72}Ge والسيلينيوم ^{74}Se

تم اجراء حسابات عوامل التشكل و CDD في اطار نموذج القشرة في مساحة النموذج $1f_{5/2}$, $2p_{3/2}$, $2p_{1/2}$ and $1g_{9/2}$ من خلال استخدام التفاعل الفعال jun45

ينتج عن جعل الهاملتونيان قطريا والذي يستفيد من التفاعل الفعال jun45 للحصول على الدوال الموجية لفضاء الانموذج .

تم استخدام تفاعل سكيرم الفعال مع معلمات (Sk35-Skzs*) في حساب عوامل التشكل باستخدام الدالة الموجية لفضاء الانموذج الناتجة عن تداخل جميع الدوال الموجية الناتجة عن خلط التشكيلات لجميع حالات فضاء الانموذج المعتمدة دون اي قيود مفروضة على فضاء الانموذج

تمت مقارنة نتائج $|F_{C0}(q)|^2$ وCDD بالبيانات التجريبية المتاحة وتبين ان حسابات فضاء الانموذج بدون اي تقييد قادرة على وصف عوامل التشكل و CDD لجميع دراسة النوى تم اجراء هذه الحسابات ضمن نهج هارتري –فوك بالاقتران مع تفاعل سكيرم الفعال .

Republic of Iraq
Ministry of Higher Education
& Scientific Research
University of Babylon
College of Education for Pure Sciences
Department of Physics

Nuclear Structure Study of Some Selected Nuclei Near Core ^{56}Ni by Using Skyrme-Hartree Fock Interaction

A Thesis
Submitted to the Council of College of Education for Pure Sciences, University of Babylon in Partial Fulfillment of the Requirements for the Degree of Master in Education/Physics

By

Nawras Taleb Sheehab Ahmed

(B.Sc. in Physics, University of Babylon, 2002)

Supervised by

Prof. Fouad A. Majeed , Ph.D.
College of Education for Pure Sciences
Department of Physics

2022 A.D. **1444 A.H.**

﴿ وَأَنزَلَ اللَّهُ عَلَيْكَ الْكِتَابَ وَالْحِكْمَةَ وَعَلَّمَكَ مَا لَمْ تَكُن تَعْلَمُ وَكَانَ فَضْلُ اللَّهِ عَلَيْكَ عَظِيماً ﴾

النساء / الآية (113)

dedication

To my parents for their endless love, support and encouragement

For those whose love flows in my veins and always resides in my heart

to my children

To my beloved brothers and sisters

to all my teachers

Whoever gives me confidence and success finally, I dedicate this humble work

✍
Nawras T. Sheehab

Acknowledgements

First of all I have to thank ***God*** *for giving me health and strength to conduct this research.*

I would like to express my heartfelt thanks to my supervisor, ***Prof. Fouad A. Majeed****, for the encouragement, valuable guidance, helpful advice and efforts that went into preparing this work.*

I would like to express my deep thanks to the ***Dean of the College of Education for Pure Sciences and the Head of the Physics department of physics at University of Babylon*** *for their assistance in completing this work…*

✍
Nawras T. Sheehab

Abstract

Finding the charge distributions and transition densities of nuclus is made possible via electron scattering. Short-lived neutron-rich nuclei will soon have access to this tool. In the present study, the elastic electron scattering C0 form factor $|F_{C0}(q)|^2$ and the charge density distribution (CDD) have been investigated for the 0^+ ground state of Nickel ^{58}Ni, Zinc ^{64}Zn, Germanium ^{70}Ge, Germanium ^{72}Ge, and Selenium ^{74}Se nuclei.

The calculations of the form factors and CDD is performed in the framework of the shell model in the model space $1f_{5/2}$, $2p_{3/2}$, $2p_{1/2}$ and $1g_{9/2}$ by utilizing jun45 effective interaction.

The diagonalization of the Hamiltonian, which makes advantage of the jun45 effective interaction, yields the wave functions for the model-space.

The Skyrme effective interaction with (Sk35-Skzs*) parametrization is used in the calculation of the form factors using the model space wave function generated from the overlapping of all the wavefunctions resulted from configuration mixing of all the states of the adopted model space without any restrictions imposed on the model space.

The results of $|F_{C0}(q)|^2$ and CDD were compared with the available experimental data and it show that the model space calculations without any truncation are capable to describe the form factors and CDD for all the studied nuclei.

These calculations were carried out within the Hartree Fock approach in combination with Skyrime effective interaction

List of contents

No	subject	Page no.
List of Figures		**I**
List of symbols and abbreviations		**II**
Chapter one: General Introduction		
1.1	introduction	1
1.2	Literature Survey	7
1.3	Aims of the Work	12
Chapter Two: Theoretical Background		
2.1	Introduction Shell Model Formalism	13
2.2	Tassie Model (TM)	19
2.3	Bohr-Mottelson Collective Hamiltonian	22
2.4	Skyrme's successful interaction	26
Chapter Three: Results and Discussion		
3.1	Introduction	29
3.2	Results and discussion	29
3.2.1	^{58}Ni nucleus	30
3.2.2	^{64}Zn nucleus	32
3.2.3	^{70}Ge nucleus	34
3.2.4	^{72}Ge nucleus	36
3.2.5	^{74}Se nucleus	38
Chapter four: conclusions, suggestions for future work		
4.1	Conclusions	41
4.2	Suggestions for future work	42
References		43
Appendix		53

List of Figures

NO.	Figure	Page no.
3.1	(A) the distribution of the charge density for the ^{58}Ni nucleus by utilizing Skyrme parameterization "Sk35-Skzs*".	31
3.1	(B) C0 charge form factor for the $\mathbf{0_1^+1}$ state in ^{58}Ni nucleus**.**	32
3.2	(A) the distribution of the charge density for the ^{64}Zn nucleus by utilizing Skyrme parameterization "Sk35-Skzs*".	33
3.2	(B) C0 charge form factor for the $\mathbf{0_1^+1}$ state in ^{64}Zn nucleus**.**	34
3.3	(A) the distribution of the charge density for the ^{70}Ge nucleus by utilizing Skyrme parameterization "Sk35-Skzs*"**.**	35
3.3	(B) C0 charge form factor for the $\mathbf{0_1^+1}$ state in ^{70}Ge nucleus.	36
3.4	(A) the distribution of the charge density for the ^{72}Ge nucleus by utilizing Skyrme parameterization "Sk35-Skzs*"**.**	37
3.4	(B) C0 charge form factor for the $\mathbf{0_1^+1}$ state in ^{72}Ge nucleus.	38
3.5	(A) the distribution of the charge density for the ^{74}Se nucleus by utilizing Skyrme parameterization "Sk35-Skzs*"**.**	39
3.6	(B) C0 the charge form factor for the $\mathbf{0_1^+1}$ state in ^{74}Se nucleus.	40

List of symbols and abbreviations

Symbol or Abbreviation	Meaning
$U\ (ri)$	Otential energy
ω	Oscillator's angular frequency
$W\ (\vec{r}_k\ ,\vec{r}_\ell)$	Two-body interaction
q	Momentum transfer
T_i	Kinetic energy
r	Radial distance.
TM	Tassie model
$\rho_0(i,f,r)$	Represent the ground state chare density
α	Represents the fine structural constant
(Sk35-Skzs*)	Skyrme parameterization
C0	Coulomb mutlipolarity operator for the ground state
$\hat{k}^2, \hat{\acute{k}}^2$	Relative momentum operators
$\vec{q}$	Three- momentum transfer
Z	Atomic number of the nucleus
Ze	Charge of nucleus
CDD	Charge density distribution
$F_J^L(q)$	Longitudinal form factor
CP	Core polarization effects
NN	Nucleon- nucleon interaction
HO	Harmonic oscillator
B	Size parameter
M	Mass of the target
q_μ	Four momentum transfer
Ω	Angular frequency
T	Total isospin
T_z	Projection isospin
L	Orbital angular momentum quantum number
J	Total angular momentum
e	Electron charge
n!	Factorial of n
n!!	Double factorial of n
$\hat{T}^L_{p/n}$	Single particle operator for proton/neutron
OBDM	One-body density matrix
$a^\dagger$	Creation operator
$\grave{a}$	Annihilation operator
$\hat{\rho}(\vec{r},t_z)$	Nucleon charge density operator

$\hat{T}^{L}_{JMt_z}(q)$	Longitudinal operator
$j_J(qr)$	Spherical Bessel function
$\delta(\vec{r}-\vec{r}_i)$	Dirac delta function
rms	Root mean square charge radii
b_{rms}	Length parameter
$F_{c.m}(\vec{q})$	Center of mass form factor
$F_{f.s.}(\vec{q})$	Form factor due to the nucleon- finite size
q_{eff}	Effective momentum transfer
A	Atomic number of nucleus
MS	Model space
$\rho_J^{ms}(i,f,r)$	Model space charge density
H	Hamiltonian of the many particles system
$f(r)$	Connected to the central potential
$H^{(0)}$	Unperturbed Hamiltonian
$\hat{P}_\sigma$	Spin exchange operator
V	Free nucleon –nucleon interaction
$\hat{\sigma}$	Representing the Pauli spin matrices
K	$K = 2\pi/\lambda$, wave vector or propagation vector
PWPA	Plane Wave Born Approximation
DWBA	Distrorted Wave Born Approximation
$U(r)$	Woods-Saxon potential
$W_0, \alpha, t_0, t_1, t_2, t_3, x_0, x_1, x_3$	The Skyrme parameterizations
$R_{nl}(r)$	Radial part of the single-particle wave function
R_0	Nuclear raduis
r_0	Raduis =1.44 or 1.2
NuShellX	Shell model code Written by Bill Rae
NuShellX@MSU	Shell model code by B. Rae and B. A. Brown
GXPF1A	Effective interaction
M1, E2	Magnetic and electric multipoles
OBTD	One-Body Transition Density
J^π	Total angular momentum with selected parity (π)
SKX	Skyrme-Hartree Fock potential
$\Phi^{core}_{J,\tau}$	Wavefunctions For core
$\varphi_{\alpha 1}$	The single-particle wavefunctions
HFB	Hartree-Fock Bogoliubov
$U_{(r_k)}$	Average potential
(β,γ)	The quadruple deformation
E_{core}	Represents the binding energy of the core

CHAPTER ONE :
General Introduction

Chapter One
General Introduction

1.1 Introduction

Many theoretical and experimental works have lately centered on the structure of neutron-rich nuclei. The anticipation that significant changes can be made to the inherent shell structure of nuclei with a significant neutron excess is at the heart of the ongoing inquiry[1]. Recent experimental and theoretical research has focused on the far from the stability valley are neutron-rich fp-shell nuclei [2,3,4].

Shell structure of nuclei with a significant excess of neutrons [5] . In order to provide a meaningful description of such nuclei, it is essential to recognize the activities that causes changing in nuclear shell form as the amount of neutrons in nuclear system increases. Traditional magic numbers (the numbers 2, 8, 20, 28, 50, 82, and 126) , which have been shown to exist in stable nuclei, have been questioned by theoretical simulations [6] .

Over the last fifty years, various nuclear models have been adopted. One such nuclear model, the nuclear shell model, has been very successful in describing nuclear structure and which continues to provide the main theoretical tool for understanding the properties of nuclei. It can be used in the simplest single particle form to provide a qualitative understanding. However it is also used as a basis for more complex and complete computations[7], these explains a great deal of the properties of nuclear energy levels. The mobility of each nucleon, according to the nuclear shell model, is dictated by the sum the others" nucleons' average " attractive forces.

The resultant orbitals shape "shells" that resemble the orbitals of atom's electron. As nucleons are added to the nucleus, they drop into the lowest-energy shells permitted by the Pauli Principle (according to the

Pauli exclusion principle, no more than one nucleon can occupy a quantum state). It calls for a distinct set of quantum numbers to characterize the motion of each nucleon. An incredibly stable nucleus occurs after a shell was fully formed (that's also, whenever the nucleons have exhausted all possible principal quantum assessment collections). This is comparable to the idea that an atom's entire set of electron quantum numbers provides it amazing stability, making it an inert gas[8].

The number of neutrons or protons in a nucleus when all of them are in filled shells is referred to as the "magic number." are mystical. J, the total angular momentum, is 0 for full shells. The following additional nucleon identifies J as the beginning condition of the new ground state (a valence nucleon).

The parity and isospin projection quantum numbers, as well as the angular momentum, are modified after nucleons (individually or in pairs) are awakened out of the situation of being on the ground state. The shell model explains how the quantum numbers differ and what energy is required to move a nucleon through one orbital to another. excited nuclear states decay into more stable nuclear states, or more stable nucleon orbitals[9] .

When the nucleons have assigned every conceivable quantum number, a stunning stable nucleus arises. Complex alpha, beta, and gamma detectors and related electrical circuitry are needed for detecting the rates at which nuclear energy levels shift in order to determine the energy and half-life of the decay. Nuclear physicists may use the transition probability (or decay rate) between nuclear states which is calculated using quantum mechanics and the shell model theory. The molecular orbital estimations conclude surprisingly very well evaluated spin and parity tasks, and also transformation probabilities, for nuclei

whose formation could be explained by several valence nucleons beyond the full shell [5].

It is the "shell model" that cornerstone for nucleon-based simulations of nuclear structures. This paradigm, which initially arose in nuclear physics almost half a century ago, is still in use today [5,6], the shell model plays a prominent role, due to the fact that it is a basic structure that relies on fewer assumptions, and because of this, it has proven to be very effective in roughly describing the low excitation energy of light nuclei, each nucleus within a spherical potential with an important rotational component, the nucleus begins to move independently of these [10] .

Calculations for the nuclear shell model, which are performed without the application of scaling factors, the observed static moments or transition strengths cannot be reproduced in Model Space (MS), where the nucleons are constrained to a small number of orbits. To match the experimental results, the matrix must be scaled to account for faults in the shell model wave functions that arise when the one-body operators are multiplied by effective charges. Effective charges, on the other hand, may bring computed transition strengths although non-zero momentum transfer (q) values may diverge greatly from observed values; they are calculated at the photon point, in addition to form factors at the first maximum whose values are closest to observed ones[11] .

In the lack of an explicit solution to the n-body issue, most scientists believe that the interacting shell model is the most basic way to understand the nucleus. with the residual interaction between the valance nucleons playing a crucial role[12] .

Electron scattering has been shown to be effective. One of the greatest methods to discover the characteristics of the energy levels of atomic nuclei [13]. where electron scattering from the nuclei provide the

most accurate data on nuclear size and charge distribution, as well as crucial information on electrodynemically currents within nuclei. Since electron scattering is sensitive to charge and the spatial dependence of current density, it can be an excellent test for such calculations [14,15].

For a variety of reasons, electron scattering is a successful method for the purpose of examining nuclear structure. Because the electrons interact electromagnetically with the charge and current density of the nucleus; The interaction is small and well known. Measurements can be made without causing significant damage to the structure of the target nuclei [16].

On the other hand, nucleons do not have a recognized structure or interaction, which makes it impossible to distinguish between them, using electron scattering to compare experiment results, without significantly disturbing the structure of the target nucleus[17].

The nuclear structure can be inferred from the high-energy electron scattering from the nucleus by using the de Broglie wavelength magnitude associated with the electron. The de Broglie wavelength lies within the spatial extension of the target nucleus when the energy of the incoming electron is more than 100 MeV. As a result, at this energy, the electron is the most effective probe for evaluating the elements of the nuclear structure allowing direct access to the target nucleus structure without significantly altering it, from local charges and current density operators[18].

There are three types of scattering experiments. First, the particle in which the falling particle interacts with the nucleus only by electromagnetic interaction, such as rapid electron scattering, and does not feel the nuclear forces. It can give us information about freight and density.

Second, we may learn about particle density from the scattering of electrically neutral particles, such neutrons, which only interact with the nuclear field. Lastly, electrically charged particle dispersion Strong nuclear interactions are also experienced by charged particles like protons and alpha particles [19] .

The other benefit of electron scattering is that they may adjust the three-momentum transfer and energy transfer independently for a given energy loss to the target [20]. The scattering of nucleons from nuclei, on the other hand, is poorly understood, It is challenging to discern between their effects in data analysis when neither the reaction nor the formation of the aim are recognized. There are two types of electron scattering: in the first, referred to as "elastic electron scattering," the nucleus is left in its ground state. The nucleus is left in its many excited states in the second kind, which is known as "Inelastic Electron Scattering" [21] .

We can discover more about the distributions of charge and magnetization in static nuclear characteristics via elastic electron scattering. It is possible to detect multipolarities and parties of transitions using inelastic electron scattering, and nuclear dynamics may be studied using transition densities [22] .

The first Born approximation may be used to describe electron scattering is a momentum-carrying exchange of virtual photons between the electron and the nucleus. The initial Born approximation holds true only if $Z\alpha \ll 1$, where Z represents the atomic number and α represents the fine structural constant. There are two forms of electron scattering from the nucleus identified by this approach [23].

The first investigation of the electron scattering was due to Mott made the initial investigation of electron scattering in 1929 by calculating the cross section of such scattering from a charge point nucleus called a Ze [24]. By a factor dependent on the charge, current, and magnetic

distributions of the target nucleus, known as the nuclear form factor, the Mott cross-section can be multiplied to calculate the nuclear size. The incident and scattering electron energies as well as the scattering angle can be used to experimentally calculate the form factor as a function of nucleus momentum transfer ($\vec{q}$)[25] .

form index was classified into two types:

1. "The longitudinal form factor carries the angular momentum of the virtual photon". The virtual photon's transverse form factor has an angular momentum of 1.
2. The transverse form there are two parts to the transverse form factor: magnetic (M) and electric (E) .

Nuclear size and density distribution are the fundamental parameters that characterize nuclear characteristics [23,24].

Experimentally determining transition densities, the charge density distribution (CDD), and form factors—all significant characteristics of a nucleus—are all made possible by the nucleus's ability to scatter high-energy electrons. The data acquired in these investigations is more exact the more momentum conveyed to the nucleus [24] .

Even though start charging density are inextricably linked to the wave equation of proton, that were critical key factors for several nuclear physics calculations, those who would provide a great deal of data about the internal structures of nuclei. Among the most effective methods for the analysis nuclear charge density is electron nucleus scattering. This technique has been used to examine the charging density dispersion of steady nuclei [22,26].

In the model space, perturbation theory-derived effective operators may be used to account for core-polarization (CP) effects. Around fifty years ago, inconsistencies between the basic shell model's predictions and actual values for nuclear magnetic moment, quadruple

moments, gamma-transition rates, and other parameters were reported in the scientific literature for the first time [26] .

There were many efforts to establish a plausible model for calculating the CP effects. Tasmanian Model [27],valence model [28] in addition to the Bohr-Mottelson model [29] are a few of these tries. Several groups have employed first and second order perturbation theory to account for the CP effects.

1.2 Literature Survey

Structure of the nucleus has piqued curiosity during the last century, and the following are some of the topics that are relevant to the current work:

In 2000, S. Ghugre and S. Chintalapudi,[30] Coincidence model calculations were performed in the lower fp shell region (for nuclei ^{44,45}Ca and ^{47}Sc), using different model tracts, to explore the effect of mixing composition from $p_{3/2}$, $p_{1/2}$ and $f_{5/2}$ orbitals on the dominant ($f_{7/2}$) n states. and the contribution arising from excitation N = Z = 16 core. Calculations indicated that excitation of nucleons via N = Z = 16 magic shell closure contributes significantly to the wave functions of the observed plane structures of ^{44,45}Ca nuclei.

In 2001, **R. Radhi, *et al.*** [31], studied the inclusion of the effects of core polarization while analyzing the Coulomb form factors of the p-nuclei for C2 transitions. For central polarization calculations, it supports up to six high-energy excitations. They found that the initial polarization affects the strength of the transmission and the dependence of the momentum transfer on the form factors, and that this function is in agreement with the observed data without movable parameters.

In 2002, **R. Radhi** [32], used microscopic theory to incorporate the effect of high formations outside the s.d. "shell model space", known as the first high fundamental polarizing effect, which allows the activation of particles and holes from 1s and 1p shells. 1d and 1f-2p primary orbits with two sparks. A baseline polarization effect was needed to characterize the information without changing parameters.

In 2003, R. Radhi [33]**,** explored Coulomb form factors for single-particle quaternary transformations. Basic orbital excitations up to higher orbitals have been combined with two excitations in a microscopic theory involving basic polarization effects. superficial changes. As a residual reaction, delta was used. The transitions ($1p_{11/2}$ $1p_{13/2}$) were processed in ^{15}N, ($1d_{5/2}$ $2s_{1/2}$) in ^{17}O, and ($1d_{13/2}$ $2s_{11/2}$) in ^{39}K. Inclusion of basic polarization effects influence the form factors and adequately represent the results of the experiment information in terms of total power and motion transmission dependency.

In 2004, **N. Smirnova, *et al.*** [34], examined differences in the nuclear field, in neutron-rich nuclei, from the nuclear shell model. The change has been identified as originating mainly from the unipolar part of Effective interaction between a proton and a neutron binary. Applications for low countries in the stranger Copper cores were studied. The results were compared used both schematic and realistic powers and comparing unipolar transitions with results obtained from large-scale chance model calculations.

In 2005, **B. Danilin, *et al.*** [35]**,** studied of charge form factors for several unstable neutron-rich isotopes of light, Medium and heavy nuclei (He, Li, Ni, Kr, Sn) were shown and compared with those of the stable isotopes. in the same isotopic series. For lighter isotopes proton and neutron densities obtained by a microscopic large-scale shell model

Shape factors are proposed as predictions for future experiments on electronic radioactivity

In 2006, **Ying F. and Z. Ren.** [36]**,** used the relative mean field model with the parameters TM2 and NL-SH to calculate the $^{26-32}$S and $^{22-28}$Si binding energies and the root-square radius. The calculated results match the experiments. An ingenious approximation of form factors and an experiment with differential electronic dispersion cross-sections.

In 2007, **R. Radhi** [37], examined the form factors of inelastic electron scattering away from the closed sd shell. According to the multi-particle configuration mixing shell model, the lower states of ^{29}Si were characterized as the ^{16}O core as well as thirteen cores scattered throughout the entire sd shell orbitals.

In 2008, **Roca-Maza *et al.*** [38], compared elastic electron scattering by nuclei to measurements in stable isotopes using varying effective Skyrme force charge density and Lagrangians to identify nuclear ground states. A modified version of ELSEPA was used in Dirac's part-wave calculations. It was studied how the neutron-rich isotopes of the chains of calcium and tin isotopes differ from the neutron-deficient isotopes.

In 2009, **Moreno, *et al.*** [39], used a self-consistent axial approximate mean with density-dependent Skyrme interactions to generate ground state wave functions for the investigation. Various isovector Coulomb form factors have been used in previous calculations of the chance model to determine the inconsistent valence asymmetry.

In 2010, Goriely, *et al.*[40]**,** three new Hartree-Fock-Bogoliubov (HFB) group models, named HFB-19, HFB20 and HFB-21, were built with unconventional Skyrme powers containing t_4 and t_5 terms, that is, density-dependent generalizations of the usual t1 and t2 terms. , Straight . Latent new forces

These models were successively fitted to three different realistic equations for the state of neutron matter
whose symmetry energy density dependence ranges from very weak to Too harsh, thus reflecting our current lack of complete knowledge of high intensity behavior of nuclear material. All non-physical instabilities of nuclear matter, including the transition to polarization state in neutron star matter, eliminated by the new forces. At the same time
The new models fit essentially all available mass data with rms deviations of 0.58 MeV and It gives the same high quality that fits the measured charge radii of the previous models Skyrme's traditional forces.

In 2011, A. Hamoudi, [41]**,** considered the distortion in nuclear collective modes to be equivalent to the conversion charge density. Using this conversion charge density, the inelastic shape variants "C2 and C4" were longitudinally determined ^{20} Ni, ^{24} Mg, ^{28} Si and ^{32} Se. In this study, the basic polarization transfer density was estimated using the Tassian model and the two-state (2BCDD's) body charge density distributions.

In 2012,A. Hamoudi, *et al.* [42]**,** used a coherent density oscillation model to calculate the nucleon motion distribution in ground states (NMD) and electron-elastic scattering forms "1p-shell nuclei" variants with "Z=N", such as "^{6}Li, ^{10}B, ^{12}C, and ^{14}N nuclei (CDFM)". Nucleon density dispersion (NDD), which was calculated using both theory and experiment, served as the basis for the weight function.

In 2013, R. Radhi, A. Hamoudi [43]**,** examined the parameters of the inelastic electron scattering shape to 2^{+} and 4^{+} states at ^{46,48,50}Ti under the chance model. Both extended MS 6 and MS "($0f_{7/2}$,$1p_{3/2}$.$0f_{5/2}$,$1p_{1/2}$)" were used for the calculation. The experimental results were compared with longitudinal form factor estimates that fully explain the effects of CP.

In 2014, **L. Exotic.** [44], used the NuShellX@MSU code. Linked to ENSDF data files for automated energy level comparisons. Spectral

factors, dichotomous transport amplitudes, nuclear moments, gamma decay, and beta decay can be predicted using operator interferences.

In 2015, Al-Sammarraie *et al.* [45]**,** assumed electron scattering parameters for a ^{25}Mg core using USDA-derived single-body density matrix components. For all cases in the first series, the longitudinal form factor calculations generated high agreement, while the predictions of the chance model yielded divergent results for the exciting cases in the second sequence.

In 2016, F. Majeed, [46]**,** examined the shape factors for the transverse inelastic dipole electron scattering in ^{48}Ca using a nuclear envelope model at Ex = 10.23 MeV, an "ambiguity state" with possible variables including effective interaction, finite occupancy, and core polarization interaction. ^{40}Ca will be used as an inert nucleus, and four orbitals with eight particles have been deployed in the space of the 2p1f model and finite to ensure that this form of the transition is safe.

In 2017, Abdullah [47], used parameter MSK7, to study the Skyrme-Hartree-Fock (SHF) method ^{6}He, ^{11}Li, ^{12}Be and ^{14}Be using skyrme. Protons and neutrons, material density distribution, rms radii, nucleon binding energy, and charge shape variables are all terrestrial properties. These measurements revealed the long tail of the corona nucleus.

In 2018, Radhi, *et al.* [48], used the Skyrme-Hartree-Fock (SHF) method with MSK7 Skyrme parameter to investigate ground-state properties of the two-neutron halo nuclei ^{6}He, ^{11}Li, ^{12}Be, and ^{14}Be. These are ground state properties it includes the proton, neutron, and matter density distributions, the corresponding rms radii, and the binding energy for each nucleon and charge form factors.

In 2019, Salman, *et al.* [49]**,** extracted the inelastic longitudinal electronic scattering agents to the 2^{+} state at ^{64,66,68}Zn in the space of the "F5P shell model" with the active interaction of F5PVH. Calculation of

the Wave Objectives of the Fundamentals of a Radial Single Particle Array with a Harmonic Oscillator Potential. Results were obtained using CP and NUSHELL.

In 2020, Al-Rahmani1 [50], examined the mortar's variable width with segmented occupation numbers for the cases 2s, 2p (pound shells) and 1 g, 1 h (capture shells).

In 2021, C. Chena, [51]**,** used the Quar, Dequark continuous method of relativistic quantum field theory in order to unify the axial and induced nic pseudo-form factors, GA and GP, with the G5 pseudo-form factor or, alternatively, the GNN-leading nucleon form factor.

In 2022,M. Kortelainen *et al.* [52], used the quantum motion of protons and neutrons to change the local directions of the radii of nuclear charge. As a function of N= 28, a global pattern can be seen in the reported differential charge radius RC2> between the neutron numbers N = 28 and N = 40.

1.3 Aims of the Work

The present study aimed to investigate the inelastic electron scattering charge form factors and charge density distribution (CDD) for some selected nuclei ^{58}Ni, ^{64}Zn, ^{70}Ge, ^{72}Ge and ^{76}Se, lying in the ($1f_{5/2}$, $2p_{3/2}$, $2p_{1/2}$ and $1g_{9/2}$) model space by utilizing the jun45 effective interaction. The calculations will be performed by means of model space only by employing Tassie, Bohr-Mottelson models using the Skyrme effective interaction.

CHAPTER Two: Theoretical Background

Chapter Two

Theoretical Background

2.1 Introduction Shell Model Formalism

Any quantum mechanical problem will often entail some form of Schrodinger equation solution. Determining a suitable Hamiltonian is one of the most crucial processes. In a many-body issue such as the one encountered in nuclear physics, there are several solutions. Beginning with the assumption of independent particle motion allows the Hamiltonian to be expressed as the sum of the individual components of each particle in the nucleus [53] .

$$H^{(0)} = \sum_{i=1}^{A}[T_i + \mathrm{U}\ (\mathrm{ri})] \quad \text{---------- (2.1)}$$

where $H^{(0)}$ is the unperturbed Hamiltonian, T_i is the kinetic energy, and $U\ (ri)$ is the potential energy. The eigenfunctions to the above equation are given by the Slater determinant, which for a two-particle system is written as Because the Pauli exclusion principle requires that wave functions for identical particles be antisymmetric, the eigenfunctions to the above equation are given by the Slater determinant, which for a two-particle system is written as [54].

$$\varphi_{\alpha 1,\alpha 2} = \frac{1}{\sqrt{2!}}\begin{vmatrix}\varphi_{\alpha 1}(1) & \varphi_{\alpha 1}(2)\\ \varphi_{\alpha 2}(1) & \varphi_{\alpha 2}(2)\end{vmatrix} = \frac{1}{\sqrt{2!}}[\varphi_{\alpha 1}(1)\varphi_{\alpha 2}(2) - \varphi_{\alpha 1}(2)\varphi_{\alpha 2}(1)] \text{-----(2.2)}$$

where $\varphi_{\alpha 1}$are the single-particle wavefunctions, given by the product of radial and angular components. This results in an equation comprising Clebsch-Gordon coefficients, spherical harmonics, and the radial component that is rather complicated. However, the only undefined portion of this equation is the radial portion $R_{n\ell}(r)$. The shape of the

potential $U(ri)$of the eq determines the features of this function equation (2.1).

It turns out that deciding on this possibility is not an easy task. Within the confines of the nuclear radius, it must mimic the known characteristics of the nuclear force, which is short-ranged, strong, and relatively steady (i.e. a flat bottom). Harmonic Oscillator (HO) is the most commonly employed potential in this instance, despite the fact that was neither brief and not only consistent inside the nucleus' radial distance (however a modifying "HO" possibilities was generally used, that "flattens" the bottom of the possibilities).The use of a "HO" possibilities is still advantageous as for the eigen functions" $\varphi_{\alpha 1}$" are well easily integrated. However, Woods-Saxon (WS) describes a more realistic potential that vanishes at high , seems to have a flat bottom but cannot be integrated [55]

$$U(r) = \frac{1}{2} m\omega^2 r^2 \text{ (Harmonic Oscillator) ---------- (2.3)}$$

where *m* is the mass of the nucleon, ω is the oscillator's angular frequency, where the radius parameter is r [55]

$$U(r) = \frac{U_0}{1+\exp\left(\frac{r-R_0}{a}\right)} \text{ (Woods - Saxon)---------- (2.4)}$$

where U_0 denotes possible depth, a denotes diffuseness, and "$R_0=r_0A^{1/3}$". The shell gaps found in nuclear data are not replicated by plugging any of these equations into the Schrodinger equation. The inclusion of a significant spin-orbit component is required to fully account for these "magic numbers" Spin-orbit coupling is a difficult subject to grasp. The intrinsic nucleon spin generates an apparent motion of the nucleus around the nucleon from the viewpoint of only one nucleon going around the nucleus.

The magnetic moment of the nucleon interacts with the magnetic field produced by the apparent motion. Multiplying the dot products of

two magnetic moments yields the interaction energy. Because a nucleon's magnetic moment is proportional to its spin, and the magnetic field generated by the nucleus' The magnetic field created by the nucleus' apparent motion is proportional to the orbital angular momentum, since apparent motion is connected to orbital angular momentum. The interaction energy between spin and orbit must be proportional to the dot product $\vec{\ell}.\vec{S}$ [56]

$$U_{so} = f(r)\vec{\ell}.\vec{S} \quad \text{----------} \quad (2.5)$$

Where the function $f(r)$ is connected to the central potential and contains the reliance on the radial coordinate *r*. The expected value is based on experimental findings.$\langle f(r)\rangle_{n,\ell}$ was expected to be of the instruction" $-20A^{-2/3}$ MeV"[57]. The oscillator frequency determines the shell gap in the HO image" $\hbar\omega_0 \sim 41A^{-1/3}$ MeV".

With the increase in mass and angular momentum, the spin-orbit force becomes more prominent, and this is evident in equation (2.5) where the spin-orbit force in mass and angular momentum becomes higher, and in particular the HO shell gaps continue until nucleon number 20. It should be emphasized that a microscopic understanding of the quantitative features of the spin-orbit force are as yet not well understood, although its presence as a strong force is clearly required in order to reproduce the observed magic numbers.

The Slater determinant of formula was used to determine the standardized, anti symmetrized wave functions of a 2 particles consisting of exactly equal fermions equation (2.2). Since the nucleus contains both neutrons and protons that interact with one another. These wave functions cannot be used in their present form. Instead, it is useful to introduce a

new quantum number, the isospin τ (referred to later as T) [58] which facilitates the distinction between protons and neutrons. This formalism can only be employed here since protons and neutrons are so similar. Except for the Coulomb contact between protons, the nn, pp, and pn interactions are identical.

Neutrons and protons are considered various versions In the isospin hypothesis, the identical particle is assumed to have the same spin. protons having $m_\tau = -\frac{1}{2}$ and neutrons $m_\tau = +\frac{1}{2}$. The choice of $m_\tau = \mp\frac{1}{2}$ is unpredictably Because most nuclei had more neutrons than protons, the selected values were set to ensure that the majority of nuclei have positive isospin. Until far, our discussion has mostly focused on the two-particle system. It's simple to understand how the wave function's complexity skyrockets as the number of particles in a system grows.

As previously noted, determining the Slater determinant of equations is a difficult task equation (2.2) three-particle, four-particle, and other systems can be used to show this. As a result of this increasing complexity, For anything other than the lightest nuclei, the feasibility of conducting shell model calculations is jeopardized. Typically, any medium or heavy nucleus is comparable to fix this difficulty, go to the nearest double-walled container. The core is regarded as an inert system, whereas the valence nucleons are considered separately[59].

$$\Phi_{J,\tau} \sim \Phi_{0,\tau}^{core} \times \Phi_{J,\tau}(\alpha_1, \alpha_2, \dots\dots) \text{ ----------(2.6)}$$

Returning to the Hamiltonian equation (2.1), the independent Hamiltonian particle problem can now be solved by choosing *U(r).* Since circular particles interact with each other, in this case, the concept of independent particle motion seems implausible. Therefore, the two-

particle interactions that make up the independent Hamiltonian particle can be expressed as: [60]

$$H = \sum_{k=1}^{A} T_k + \sum_{k=\ell}^{A} \sum_{\ell=k+1}^{n} W\,(\vec{r}k\,, \vec{r}\ell\,) \text{ ----------(2.7)}$$

Where H is the hamiltonian of the many particles system, T_k is the kinetic energy of the and $W\ (\vec{r}_k\,, \vec{r}_\ell)$ is the two-body interaction between the k^{th} and ℓ^{th} nucleons .

The two-body interaction between the ℓ^{th} and k^{th} nucleons is denoted by $W\ (\vec{r}k\,, \vec{r}\ell\,)$ .The Hamiltonian becomes, given an average potential $U_{(rk)}$

$$H = \sum_{k=1}^{A}\left[T_k + U_{(rk)}\right] + \sum_{k=\ell}^{A} \sum_{\ell=k+1}^{n} \mathrm{W}\,(\vec{\mathrm{r}}\mathrm{k}\,, \vec{\mathrm{r}}\ell\,) - \sum_{\mathrm{k}=1}^{\mathrm{A}} U_{(rk)} \text{ (2.8)}$$

where $U_{(r_k)}$ is the average potential .

The first term is the same as the Hamiltonian for independent particles provided by equation (2.1), but the second and third terms account for the residual interaction, which is the divergence from independent particle motion. Equation (2.8) may be recast by separating the summations into core and valence contributions[61].

$$H = H_{core} + H_1 + H_2 + \mathrm{V}\,(\vec{\mathrm{r}}_1\,, \vec{\mathrm{r}}_2\,) \text{ ---------- (2.9)}$$

H_{core} comprises all nucleon interactions that make up the core, H_1 and H_2 seem to be donations from particle 1 and 2, as well as $\mathrm{V}\,(\vec{\mathrm{r}}_1\,, \vec{\mathrm{r}}_2\,)$ is the residue left reaction that identifies most reactions among particles 1 and 2 and any interconnections of core nucleons. Whenever this Hamiltonian version has been implemented to the Schrodinger formula, a similar formula for energy is obtained[62].

$$E = E_{core} + E_1 + E_2 + \left\langle \Phi_{J,\tau} \middle| \mathrm{V}(\vec{\mathrm{r}}_1\,, \vec{\mathrm{r}}_2\,) \middle| \Phi_{J,\tau} \right\rangle \text{ ----------(2.10)}$$

E_{core} represents the binding energy of the core nucleus in the preceding equation, the single-particle energies of orbitals outside the core are E_1 and E_2. and $\langle \Phi_{J,\tau} | V(\vec{r}_1, \vec{r}_2) | \Phi_{J,\tau} \rangle$ is the residual interaction. It's worth noting that equation (2.10) only gives you the energy for pure arrangements. In theory, any condition with the similar overall$(\vec{r}_1, \vec{r}_2)$ spin state and angular momentum J would then combine. Comparing calculated of wave equation combines series[63]

$$(\Psi_{J,\tau})p = \sum_{k=1}^{g} a_{kp} \left(\Phi_J, \tau\right)_k \text{ ----------(2.11)}$$

in which g seems to be the amount of structures which combine and label has been the configuration's identifier

p =1,2,..., g

So, a_{kp} coefficient satisfy the criterion,

$$\sum_{k=1}^{g} |a_{kp}|^2 = 1 \quad \text{---------- (2.12)}$$

When equation (2.11) is substituted into the Schrodinger formula, the result is :

$$H(\Psi_{J,\tau})p = E_p(\Psi_{J,\tau})p \quad \text{----------(2.13)}$$

resulting in a system of linear equations [63]

$$\begin{pmatrix} H_{11} & H_{12} & \cdots & H_{1g} \\ H_{21} & H_{22} & \cdots & H_{2g} \\ \vdots & \vdots & \ddots & \vdots \\ H_{g1} & H_{g2} & \cdots & H_{gg} \end{pmatrix} \begin{pmatrix} a_{1p} \\ a_{2p} \\ \vdots \\ a_{gp} \end{pmatrix} = E_p \begin{pmatrix} a_{1p} \\ a_{2p} \\ \vdots \\ a_{gp} \end{pmatrix} \text{---------- (2.14)}$$

Where $H_{\ell,k}$ are given by the summations of all single-particle and residual interaction terms for particles ℓ and k. A classic eigenvalue problem is represented by equation (2.14), which is solved by setting the determinant to zero

$$\begin{vmatrix} H_{11}-E_p & H_{12} & \cdots & H_{1g} \\ H_{21} & H_{22}-E_p & \cdots & H_{2g} \\ \vdots & \vdots & \ddots & \vdots \\ H_{g1} & H_{g2} & \cdots & H_{gg}-E_p \end{vmatrix} = 0$$

The perturbed energies of each state in the mixing are represented by g solutions. Each state has a unique set of coefficients a_{kp} that must be found in order to acquire the wave functions $\Psi_{J,\tau}$, hence equation (2.14) must be solved for each of the g solutions to E_p in order to obtain the coefficients a_{kp} and consequently the perturbed wave functions $\Psi_{J,\tau}$ [64] .

2.2 Tassie Model (TM)

The gamma-transition and electron excitation of nuclei have both been described using this paradigm. It's a multiple examination of inelastic scattering. The classic liquid drop model, which assumes a uniform charge distribution, is the basis for this concept. TM is an attempt to develop a more flexible model that can be tweaked to accommodate non-uniform charge and mass density distributions. The ground state density of the nucleus determines the CP transition density, according to this theory. According to the collective modes of nuclei [65] the Tassie shape, as given in equation (2.15), yields the CP transition density. For this model, the Coulomb form factor is:

$$F_J^L(q) = \sqrt{\frac{4\pi}{2J_i+1}}\frac{1}{Z}\left\{\int_0^\infty r^2 j_J(qr)\rho_J^{ms}(i,f,r)\,dr + N\int_0^\infty dr r^2 j_J(qr) r^{J+1}\frac{d\rho_0(i,f,r)}{dr}\right\} F_{f.s}(q)F_{c.m}(q) \quad (2.15)$$

Where $F_J^L(q)$ is the longitudinal form factor, $j_J(qr)$ is the spherical Bessel function, $\rho_J^{ms}(i,f,r)$ is the model space charge density, $\rho_0(i,f,r)$ represent the ground state chare density, $F_{c.m}(q) = e^{q^2b^2/4A}$ is the center of mass correction due to the lack of transitional invariance in the shell model and $F_{f.s}(q) = [1+(q/4.33)^2]^{-2}$.

The radial integral is the sum of two radial integrals.

$$\int_0^\infty dr\, r^{J+1} j_J(qr)\frac{d\rho_0(i,f,r)}{dr}$$

can be written as:

$$\int_0^\infty \frac{d}{dr}\left[r^{J+1} j_J(qr)\,\rho_0(i,f,r)\right]dr - \int_0^\infty dr(J+1) r^{J+1}\, j_J(qr)\,\rho_0(i,f,r) - \int_0^\infty dr r^{J+1}\frac{d}{dr}\, j_J(qr)\rho_0(i,f,r) \quad \ldots\ldots(2.16)$$

The second and third terms may be combined to generate the term when the first term has no effect [66]

$$-q\int_0^\infty dr\, r^{J+1}\rho_0(i,f,r)\left[\frac{d}{d(qr)}+\frac{J+1}{qr}\right] j_J(qr) \ldots\ldots (2.17)$$

Based on the spherical Bessel function's recursion

$$\left[\frac{d}{d(qr)}+\frac{J+1}{qr}\right]j_J(qr)=j_{J-1}(qr)\ \ldots\ldots\ldots(2.18)$$

$$\int_0^\infty dr\, r^{J+1}\, j_J(qr)\,\frac{d\rho_0(i,f,r)}{dr}=-q\int_0^\infty dr\, r^{J+1} j_{J-1}\,\rho_0(i,f,r)\ \ldots\ldots\ (2.19)$$

Hence, the form factor takes the form [67]

$$F_J^L(q)=\sqrt{\frac{4\pi}{2J_i+1}}\frac{1}{Z}\left\{\int_0^\infty r^2 j_J(qr)\rho_{J\,t_z}^{ms}\,dr - Nq\int_0^\infty r^{J+1}\rho_0\, j_{J-1}(qr)\,dr\right\}X\,F_{fs}(q)\,F_{cm}(q)\ \ldots\ldots(2.20)$$

where N is proportionality constant related is given by the matrix elements of gamma transitions .

The proportionality constant may be calculated using the form factor at $q=k$

$$N=\frac{\int_0^\infty dr\, r^2 j_J(kr)\rho_{J\,t_z}^{ms}(i,f,r)-ZF_J^L\sqrt{\frac{2J_i+1}{4\pi}}}{(k)\int_0^\infty dr\, r^{J+1}\rho_0(i,f,r)\, j_{J-1}(kr)}\ \text{----------(2.21)}$$

Equation (2.21) relates the factor of forms at the photon point $q=k$ to the transformation strength *B(CJ)*, which may be written as [68].

$$N=\frac{\int_0^\infty dr\, r^{J+2}\,\rho_{Jt_z}^{ms}(i,f,r)-\sqrt{(2J_i+1)\,B(CJ)}}{(2J+1)\int_0^\infty dr\, r^{2J}\rho_o(i,f,r)}\ \text{------ (2.22)}$$

with $(2J+1)!!=(2J+1)\,(2J-1)!!$

The proportionality constant is produced by adjusting the reduced transition probability *B(CJ)* with the experimental value of B using equation (2.22).

2.3 Bohr-Mottelson Collective Hamiltonian

To cogently describe quadrupole vibrations and rotations," The five-dimensional (5D) quadrupole collective Hamiltonian was created by Bohr and Mottelson". It is formatted as follows[68]:

$$H_{coll} = T_{vib} + T_{rot} + V(\beta,\gamma) \quad \text{----------(2.23)}$$

$$T_{vib} = \frac{1}{2} D_{\beta\beta}(\beta,\gamma)\dot{\beta}^2 + D_{\beta\gamma}(\beta,\gamma)\dot{\beta}\dot{\gamma} + \frac{1}{2} D_{\gamma\gamma}(\beta,\gamma)\dot{\gamma}^2 \text{----------(2.24)}$$

$$T_{rot} = \frac{1}{2}\sum_{k=1}^{3} \mathcal{J}_k(\beta,\gamma)\dot{\varphi_k^2} \quad \text{----------(2.25)}$$

Here, φ_k are the components of the rotational angle on the three intrinsic axes. The quadruple deformation (β,γ) and the rotational angles φ_k are treated as dynamical variables, and (β,γ) and $\dot{\varphi}_k$ represent their time-derivatives. The $\dot{\varphi}_k$ are called angular velocities. The quantities $(D_{\beta\beta}; D_{\beta\gamma}, and\ D_{\gamma\gamma})$ appearing in the kinetic energies of vibrational motion, T_{vib}, represent inertial masses of the vibrational motion. They are functions of $\beta$and γ.

The large amounts $\mathcal{J}_k$ (β,γ)in the rotational energies T_{rot}represent the mass moment of inertia with respect to the inherent (body-fixed) axis. The inherent axes can be determined using the primary axes of the body fixed frames which was coupled to the immediate form of the time dependent average field. V (β,γ) seems to be a term that represents possibility energy as a result of β and γ [69] .

When addressing the liquid drop model, the "Bohr-Mottelson collective Hamiltonian " equation (2.23) was frequently mentioned. The relationship between the classical liquid drop and lower frequencies quadrupole collecting motion, on the other hand, is inconsequential. The nucleus was described as a quantum fluid that has been idealized in a way that isn't seen and a really intriguing new kind of material as early as

the 1950s [69] .Since the majority of nuclei are superfluids with a radius of a few femtometers nuclear deformation differs fundamentally from surface form oscillations in a traditional liquids drop in that it can be connected to quantum structures as well as sudden trying to break of spherical symmetry in the self-consistent average field.

The form of the collective Hamiltonian (2.23) is quite general and applicable to various finite many-body systems, but the specific dynamical properties of the system of interest are revealed by the values and the (β,γ)-dependence of the collective inertia masses $\left(D_{\beta\beta}\,, D_{\beta\gamma}\,, D_{\gamma\gamma}\,, \mathcal{J}_k\right)$ as well as the potential energy $V(\beta,\gamma)$. For understanding the dynamical properties of the nucleus, therefore, it is imperative to derive these quantities in a microscopic way and compare with what experimental data indicate.

As demonstrated in this work, the collective Hamiltonian (2.23) The nucleus' low frequency quadrupole collective dynamics are astonishingly accurately represented by the collecting inertial masses and possible energy calculated by microscopic examination from the movable supercritical fluid mean field photo. Quantifying the collecting variables that keep driving the self consistent mean field's time evolution as well very well explains quantum correlation outside the mean field. The traditional Hamiltonian (2.23) has been defined in relation to the five collinear coordinate values (β ,γ) and the three Euler angles which are connected φ_k (via a linear transform) and there own duration derivative.The so-called Pauli prescription[70]

Quantization in curvilinear coordinates is possible.The Bohr-Mottelson collective Hamiltonian's microscopic derivation. This is" the quantized 5D quadrupole collective Hamiltonian"[55,57,70]:

$$\widehat{H}_{coll} = \hat{T}_{vib} + \hat{T}_{rot} + V(\beta,\gamma) \text{----------(2.26)}$$

$$\hat{T}_{vib} = -\frac{1}{2\sqrt{WR}}\left\{\frac{1}{\beta^4}\left[\frac{\partial}{\partial\beta}\left(\beta^2\sqrt{\frac{R}{W}}D_{\gamma\gamma}\frac{\partial}{\partial\beta}\right) - \frac{\partial}{\partial\beta}\left(\beta^2\sqrt{\frac{R}{W}}D_{\beta\gamma}\frac{\partial}{\partial\gamma}\right)\right] + \frac{1}{\beta^2\sin(3\gamma)}\right.$$
$$\left.\times -\frac{\partial}{\partial\gamma}\left(\sqrt{\frac{R}{W}}\sin(3\gamma)\,D_{\beta\gamma}\frac{\partial}{\partial\beta}\right) + \frac{\partial}{\partial\gamma}\left(\sqrt{\frac{R}{W}}\sin(3\gamma)\,D_{\beta\beta}\frac{\partial}{\partial\gamma}\right)\right\} \text{-------(2.27)}$$

and the rotational energies word $\hat{T}_{rot}$ was provided by [71]

$$\hat{T}_{rot} = \sum_{k=1}^{3}\frac{\hat{I}_k^2}{2\,\mathcal{J}_k(\beta,\gamma)} \quad \text{----------(2.28)}$$

with $\hat{I}_k^2$ denoting three components of the angular-momentum operator with respect to the intrinsic axes. In this paper, we use the unit with $\hbar = 1$. In the above equations [71]

$$\beta^2\,W(\beta,\gamma) = D_{\beta\beta}(\beta,\gamma)D_{\gamma\gamma}(\beta,\gamma) - D_{\beta\gamma}^2(\beta,\gamma) \text{---------- (2.29)}$$
$$R(\beta,\gamma) = D_1(\beta,\gamma)\,D_2(\beta,\gamma)\,D_3(\beta,\gamma) \text{---------- (2.30)}$$

and $D_k(\beta,\gamma)$ "$(k = 1;\ 2;\ 3)$" seem to be the rotary inertial function relating to inertial moments by[71]

$$\mathcal{J}_k(\beta,\gamma) = 4\beta^2 D_k(\beta,\gamma)\sin^2(\gamma - 2\pi k/3) \text{---------- (2.31)}$$

Unless totally inertially mass $\left(D_{\beta\beta}\,, D_{\gamma\gamma}\beta^{-2}, D_1\,, D_2\,, D_3\right)$ were replacing by a recurring constants:
D and $D_{\beta\gamma}$ was ignoring, the over head $\hat{T}_{vib}$ was decreased to [71]:

$$\hat{T}_{vib} = -\frac{1}{2D}\left(\frac{1}{\beta^4}\frac{\partial}{\partial\beta}\beta^4\frac{\partial}{\partial\beta} + \frac{1}{\beta^2\sin(3\gamma)}\frac{\partial}{\partial\gamma}\sin(3\gamma)\frac{\partial}{\partial\gamma}\right) \text{----------(2.32)}$$

Only small-amplitude Hartree-Fock Bogoliubov (HFB) equilibrium vibrations may be suitable for such an extreme

approximation. This fundamental estimate for inertia masses has been highlighted as insufficient.

The collective Schrödinger equation is [72]

$$\left(\hat{T}_{vib} + \hat{T}_{rot} + V(\beta,\gamma)\right) \Psi_{\alpha IM}(\beta,\gamma,\Omega) = E_{\alpha I}\, \Psi_{\alpha IM}(\beta,\gamma,\Omega) \text{-------- (2.33)}$$

The collective wave function in the laboratory frame, $\Psi_{\alpha IM}(\beta,\gamma,\Omega)$, is a function of β , γ and Ω set of three Euler angles Ω. It is specified by the total angular momentum I, its projection onto the z-axis in the laboratory frame M, and α that distinguishes the eigenstates possessing the same values of I and M. With the rotational wave function $\mathcal{D}^{I}_{MK}$, they are written as $\Psi_{\alpha IM}(\beta,\gamma,\Omega) = \sum_{K=even} \Phi_{\alpha IK}(\beta,\gamma)\ \langle\Omega|IMK\rangle$ ---------(2.34)

$$\langle\Omega|IMK\rangle = \sqrt{\frac{2I+1}{161\pi^2(1+\delta_{K0})}}\ \left[\mathcal{D}^{I}_{MK}(\Omega) + (-1)^I\, \mathcal{D}^{I}_{M,-K}(\Omega)\right] \text{ ------(2.35)}$$

In the body-fixed frame, the vibrational wave operates,$\Phi_{\alpha IK}(\beta,\gamma)$, are normalized as [73]

$$\int d\beta\ d\gamma\ \sqrt{G(\beta,\gamma)}\ |\Phi_{\alpha I}(\beta,\gamma)|^2 = 1 \quad \text{----------(2.36)}$$

where

$$|\Phi_{\alpha I}(\beta,\gamma)|^2 = \sum_{K=even} |\Phi_{\alpha IK}(\beta,\gamma)|^2 \text{----------(2.37)}$$

as well as the volume factor is calculated by $\sqrt{G(\beta,\gamma)}\ d\beta\ d\gamma$ with :

$$G(\beta,\gamma) = 4\,\beta^8\, W(\beta,\gamma)\, R(\beta,\gamma) \sin^2(3\gamma) \text{--------- (2.38)}$$

In the references, the symmetry of collecting wave function and boundaries condition for trying to solve the collecting Schrodinger formula have been extensively studied. We obtain the eigenvalue formula for vibrational wave function by plugging (2.34) into the collecting Schrodinger formula (2.33) [74-76]

$$\left[\hat{T}_{vib} + V(\beta,\gamma)\right] \Phi_{\alpha IK}(\beta,\gamma) + \sum_{K'=even}\left\langle IMK\left|\hat{T}_{rot}\right|IMK'\right\rangle \Phi_{\alpha IK'}(\beta,\gamma) = E_{\alpha I}\, \Phi_{\alpha IK}(\beta,\gamma) \quad \text{----------(2.39)}$$

When this formula is solved, it produces quantum spectroscopy and collecting wave features. It is so simple to determine the likelihood of electromagnetic transitions between aggregate excited states.

2.4 Skyrme's successful interaction

For HF nuclei calculations, Skyrme offered a beneficial interface. It is the most appropriate force for fitting experimental nuclei data such as binding energies and charged radii when establishing the ground conditions characteristics of nuclei with around 10 variable parameters[77].

When a momentum-dependent two-body term and a zero-range three-body term interact at zero range, the Skyrme forces are produced. In HF calculations, a density-dependent two-body component can be substituted for the three-body term. As a result, The Skyrme troops have been merged into a single, more powerful force. Skyrme explains the contact between two bodies as follows[77]:

$$v_{12} = t_0\left(1 + x_0\hat{P}_\sigma\right)\delta(r_1 - r_2) + \frac{1}{2}t_1\left(1 + x_1\hat{P}_\sigma\right)\left(\hat{k}^2\delta(r_1 - r_2) + \delta(r_1 - r_2)\acute{\hat{k}}^2\right)$$
$$+t_2\left(1 + x_2\hat{P}_\sigma\right)\hat{k}^2.\delta(r_1 - r_2)\hat{k} + \frac{1}{6}t_3\left(1 + x_3\hat{P}_\sigma\right)\rho^\alpha\left(\vec{R}\right)\delta(r_1 - r_2) +$$
$$iW_0\acute{\hat{k}}^2(\hat{\sigma}_1 + \hat{\sigma}_2)\hat{k}\delta(r_1 - r_2) \text{ ---------- (2.40)}$$

where $\delta(r_1 - r_2)$ is the Dirac delta function $\hat{k}^2$ and $\acute{\hat{k}}^2$ are relative momentum operators which operate on the wave functions to the right and to the left. Also $\hat{P}_\sigma$ is the spin exchange operator, with $\hat{\sigma}$ representing the Pauli spin matrices. The Skyrme parameterizations; W_0, α, t_0, t_1, t_2, t_3, x_0, x_1, and x_3 usually determined by fitting the nuclear structure experimental data. Each of the terms gives rise to both time-even and time-odd densities with HF equations.

$R = \frac{r_1 - r_2}{2}$ in this case and α is the Skyrme force's parameters. The $\hat{k} = (\vec{\nabla}_1 - \vec{\nabla}_2)/2i$ and $\hat{\acute{k}} = (\vec{\acute{\nabla}}_1 - \vec{\acute{\nabla}}_2)/2i$.

The right- and leftward-moving wave vectors of two nucleons are relative. Operators are conjugate complex wave functions (i.e. the complex conjugate wave functions). Considering $\acute{r}$ as a coordinate respectively. The terms t_0, $t_1, t_2, t_3, x_1, x_2, x_3$ and W_0 are free parameters that characterize the intensities of several interaction factors suited to nuclear structure data. $\hat{P}$ is operator of spin-exchange $\delta(r_1 - r_2)$. The overall energy density of a nucleus in a typical SHF model is

$$E = E_{kin} + E_{sky} + E_{coul} + E_{pair} + E_{cmv} \quad \text{----------(2.41)}$$

E_{kin} the kinetic energy of nucleons (protons and neutrons) may be determined using the formula below

$$E_{kin} = \sum_{i=1}^{A} \frac{\hbar^2}{2m_i} \int \tau_i d^3r \quad \text{----------(2.42)}$$

E_{sky} is the energy function of the Skyrme force is given by

$$E_{sky} = \int d^3r \left[\frac{b_0}{2}\rho^2 - \frac{\acute{b}_0}{2}\sum_q \rho_q^2 + \frac{b_3}{3}\rho^{\alpha+2} - \frac{\acute{b}_3}{3}\rho^{\alpha}\sum_q \rho_q^2 + b_1\rho\tau - \acute{\rho}_1 \sum_q \rho_q\tau_q - \frac{b_2}{2}\rho\Delta\rho + \frac{\acute{b}_2}{2}\sum_q \rho_q\Delta\rho_q - b_4\rho\nabla.J - \acute{b}_4\sum_q \rho_q\nabla.J_q \right] \quad (2.43)$$

ρ_q is the density of protons and neutrons in their immediate environment (depending on the amount of q), ρ is the density of the population, ρ_t is the densities of kinetic energy for protons and neutrons and J_q is the spin-orbit current density. These relationships provide them [78]:

$$\rho_q(r) = \sum_{i\sigma} |\phi(r,\sigma,q)|^2, \tau_q = (r)\sum_{i\sigma} \left|\vec{\nabla}\phi(r,\sigma,q)\right|^2,$$
$$J_q(r) = -i\sum_{i\sigma\acute{\sigma}} \phi_i^*(r,\sigma,q)[\nabla\phi_i \times \langle\sigma|\hat{\sigma}|\acute{\sigma}\rangle] \quad \text{----------(2.44)}$$

The parameters of the energy Skyrme equation are listed below[77].

$$\left.\begin{array}{c} b_0 = t_0\left(1+\frac{1}{2}x_0\right), \acute{b}_0 = t_0\left(\frac{1}{2}+x_0\right) \\ b_1 = \frac{1}{2}\left[t_1\left(1+\frac{1}{2}x_1\right)+t_2\left(1+\frac{1}{2}x_2\right)\right], \acute{b}_1 = \frac{1}{2}\left["t_1\left(\frac{1}{2}+x_1\right)-t_2\left(\frac{1}{2}+x_2\right)"\right] \\ b_2 = \frac{1}{8}\left["3t_1\left(1+\frac{1}{2}x_1\right)-t_2\left(1+\frac{1}{2}x_2\right)"\right], \acute{b}_2 = \frac{1}{8}\left["3t_1\left(\frac{1}{2}+x_1\right)+t_2\left(\frac{1}{2}+x_2\right)"\right] \\ b_3 = "\frac{1}{4}t_3\left(1+\frac{1}{2}x_3\right), "\acute{b}_3 = "\frac{1}{4}t_3\left(\frac{1}{2}+x_3\right)" \end{array}\right\}$$

Coulomb energy makes up the third component of the total energy equation. The exchange component, which contributes a little amount of energy to the Coulomb energy, aids it. This contribution is possible because to the infinite range of the Coulomb interaction. Using the following formula, the Coulomb energy can be calculated [79]:

$$E_{coul} = \frac{e^2}{2}\iint \frac{\rho_\rho(\vec{r})\rho_\rho(\vec{r})}{|\vec{r}-\acute{\vec{r}}|} d^3r d^3\acute{r} + E_{coul,exch}$$

$$E_{coul,exch} = -\frac{3}{4}e^2\left(\frac{3}{\pi}\right)^{1/3}\int \rho_\rho\,(r)^{4/3}dr \quad \text{----------(2.45)}$$

The nucleon densities (r) and $\rho_n(r)$ and may be calculated using a single particle wave function produced using HF calculations. the several generic products wave function $(\psi\ \beta\ )$in the "Skyrme-Hartree-Fock (SHF) theory "with the Skyrme forces have been composed of totally independent having to move single particles. The very next neutron and proton densities can be estimated using this method[79]:

$$\rho_q(\vec{r}) = \sum_i|\varphi_i(r)|^2 = \sum_\beta W_\beta \frac{2J_\beta+1}{4\pi} \quad \text{----------(2.46)}$$

CHAPTER THREE:

Results and Discussion

Chapter Three
Results and Discussion

3.1 Introduction

The characteristics of fp-shell nuclei can be described using a range of theoretical approaches. Such computations differ with the shell model's space being complete, the related parameters being mass dependent, and the two-matrix components being adequate in terms of experimental data [80].

The estimation of electron scattering form factors is also one of these important electromagnetic observables that need to be calculated and compared with the experimental data and represent good testing background for the large-scale shell model calculations. To perform the calculations one need mathematics, quantum mechanics theories, and nuclear shell model theories and formulae. These many issues must be programmed into a computer program to perform such a massive computations [81].

NushellX @ MSU code was used to perform the calculations, and for more details about the program, it is explained in the appendix

In the present work, five nuclei are considered in the fp-shell (^{58}Ni, ^{64}Zn,^{70}Ge, ^{72}Ge and ^{74}Se). The Jun45 interaction have been used to give the fp-shell model wave functions. The calculations presented here were performed using Bohr-Mottelson models.

3.2 Results and discussion

Table (3.1) provides a summary of the Sk35-Skzs* [81]calculation parameters. In any of the following diagrams, the solid red curve represents the findings of the Tassie computations (see Figure (3.1)). The results of the Bohr-Mottelson models shown by the solid blue curve.

Table 3.1: The parameters of the Skyrme residual interaction.

Force	Sk35-Skzs*
t_o (MeV. fm^3)	-1446.759
t_1 (MeV.fm^3)	250.852
t_2 (MeV.fm^3)	-132.993
t_3 (MeV.fm^3)	12127.649
W_o	153.054
x_o	0.329
x_1	0.518
x_2	0.139
x_3	0.018
α	1/2

3.2.1 ^{58}Ni nucleus

The calculations of the shell model have been utilized by using ($1f_{5/2}$, $2p_{3/2}$, $2p_{1/2}$ and $1g_{9/2}$) model space. Figure (3.1) panel (A) displays the charge density derived using the Skyrme parameterization Sk35-Skzs* investigated in the present study, and also the experimental charge distributions for the ^{58}Ni nucleus.

The charge form factor C0 for the state ($J^\pi T = 0_1^+ 1$) has been predicted using the Bohr-Mottelson and Tassie models, as shown in Figure(3.1) panel (B). In the calculations, the core is considered to be ^{56}Ni in which two valence neutrons outside the taken core. The calculations of the charge-density ρ_{ch} and C0 form factor for the ground state is performed using the model space wavefunction only. The results were compared with the measured values indicated a remarkable agreement with the measured data [82,83]

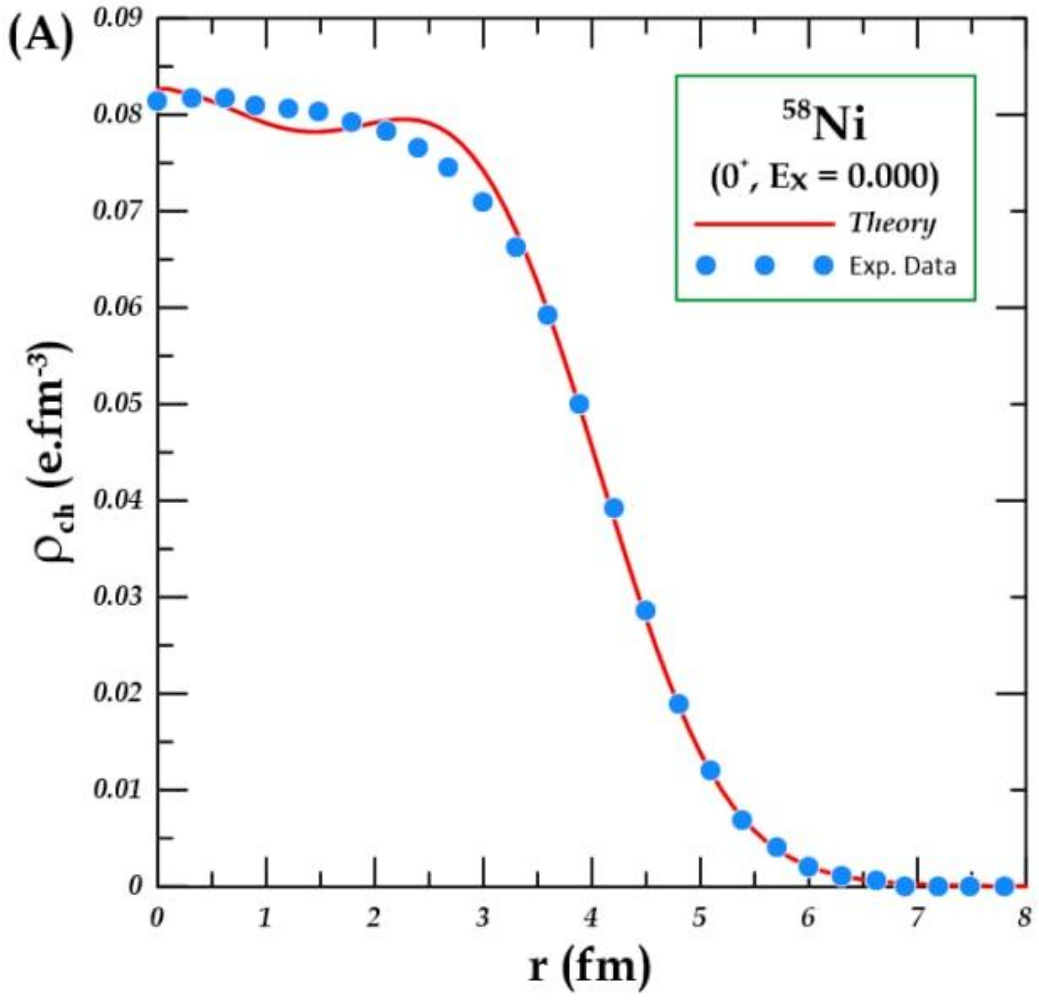

Figure (3.1): (A) The distribution of the charge density for the ^{58}Ni nucleus by utilizing Skyrme parameterization "Sk35-Skzs*", [83].

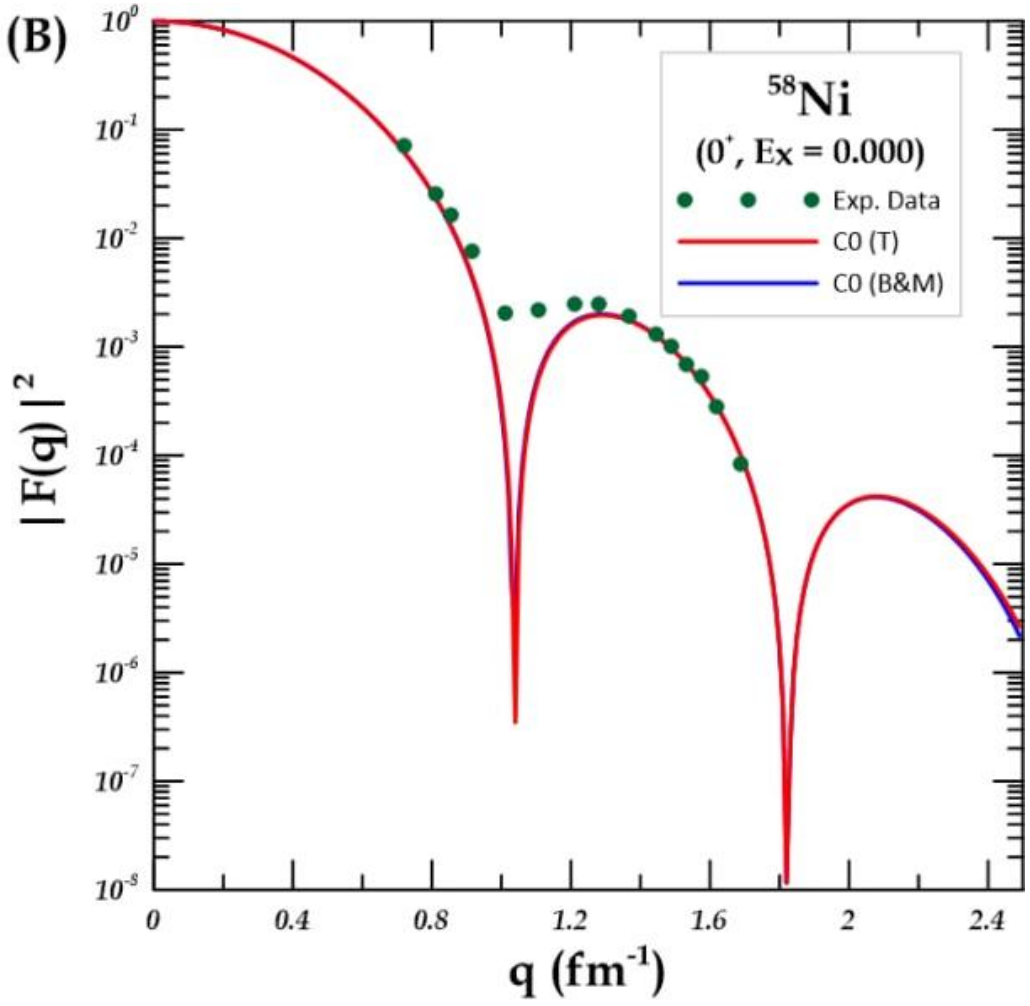

Figure (3.1): (B) Co charge form factor for the 0_1^+1 state in ^{58}Ni nucleus [83]

3.2.2 ^{64}Zn nucleus

The theoretical results of the shell model calculation were carried out using the model space ($1f_{5/2}$, $2p_{3/2}$, $2p_{1/2}$, $1g_{9/2}$) which considers ^{56}Ni core with two protons and six neutrons outside the core. The calculation is performed using the model space only. Figure (3.2) panel (A) illustrate the ρ_{ch} calculated utilizing the Skyrme parameterization Sk35-Skzs* used in this work, and the experimental charge distributions for the isotopes ^{64}Zn. The theoretical results of the ρ_{ch} were able to reproduce the experimental data. The C0 charge form factor for the ^{64}Zn nucleus is

presented in Figure(3.2) panel (B), the Tassie and Bohr-Mottelson models were used to calculate the charge form factor C0 using the effective interaction (jun45) with the shell model and the (Sk35-Skzs*) residual interaction. The calculations for both Tassie and Bohr-Mottelson models reproduce the first diffraction maxima with the of experimental data and the shape of the diffraction minima is not very clear and seems theory shifted to the high-momentum transfer [84]

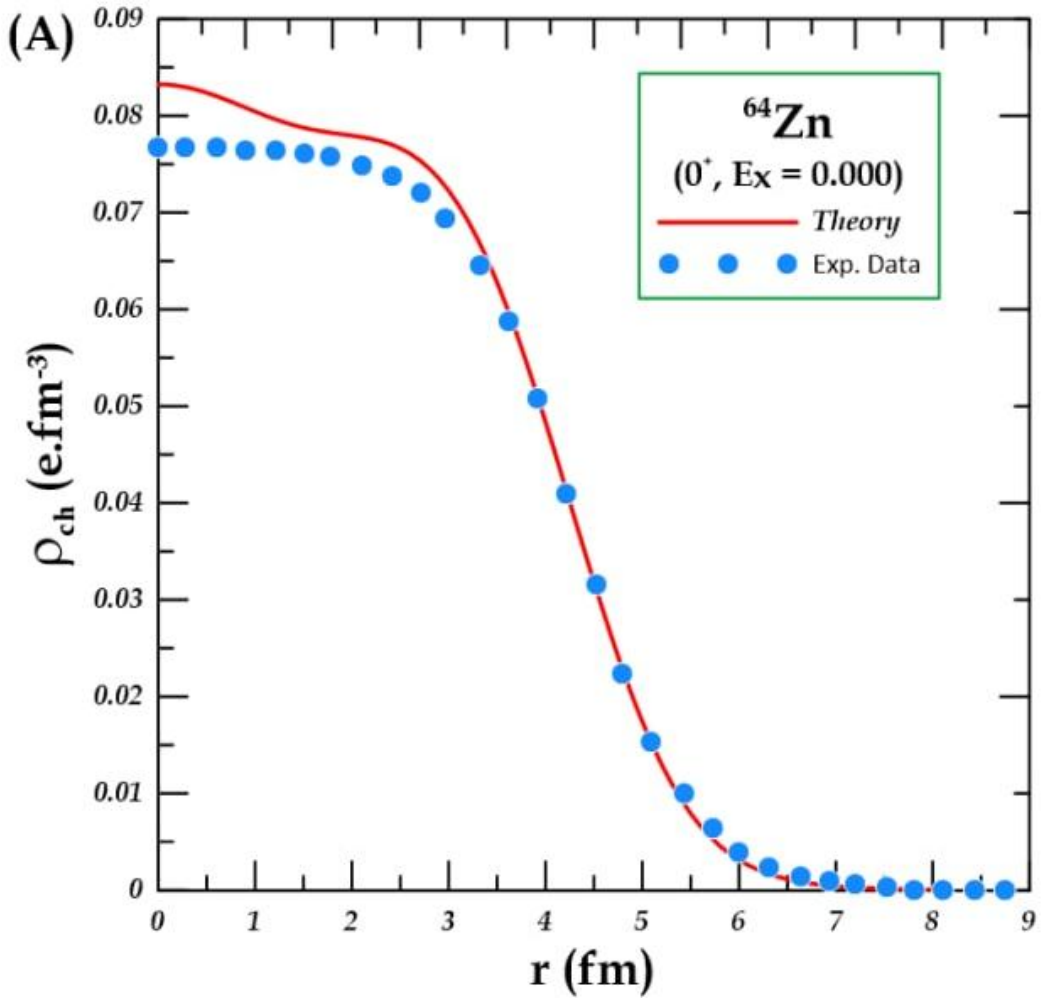

Figure (3.2): (A) The distribution of the charge density for the ^{64}Zn nucleus by utilizing Skyrme parameterization "Sk35-Skzs*", [84].

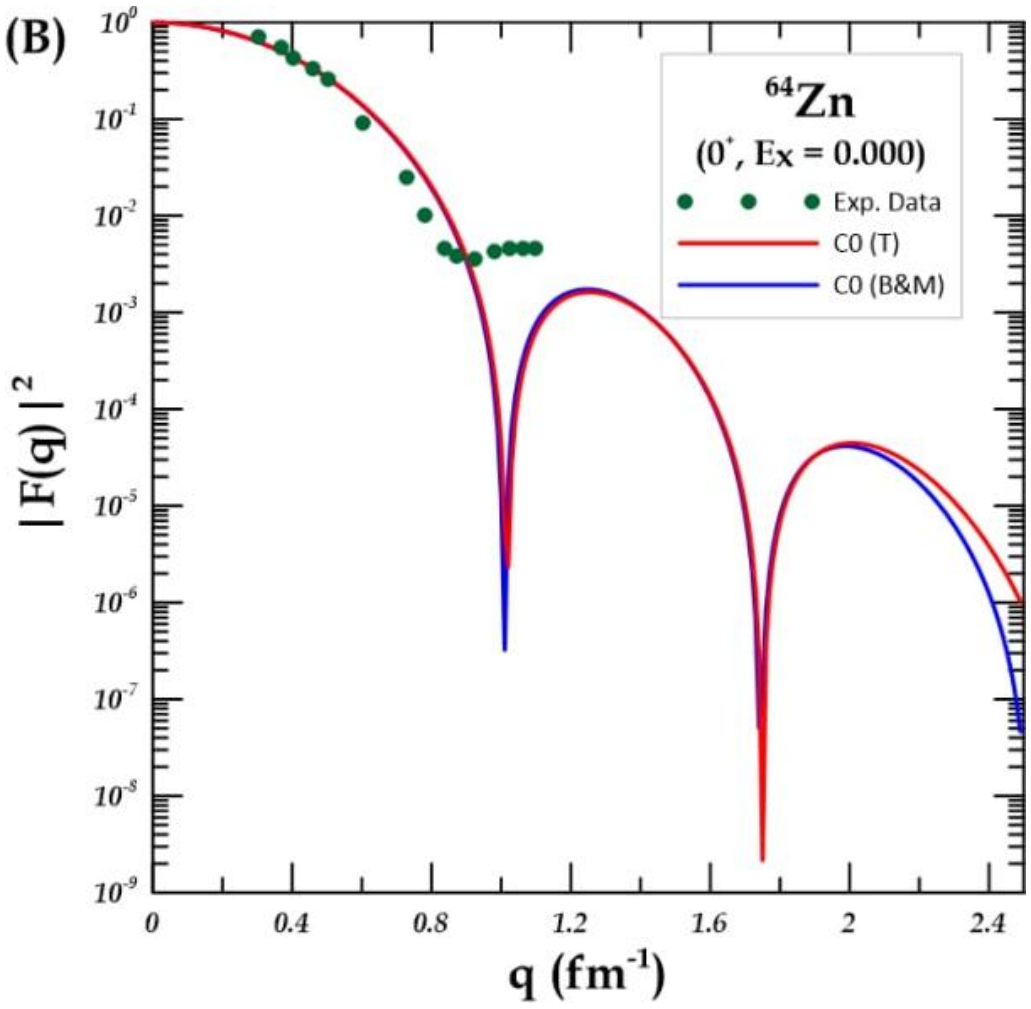

Figure (3.2): (B) C0 charge form factor for the 0_1^+1 state in ^{64}Zn nucleus, [84].

3.2.3 ^{70}Ge nucleus

Figure (3.3) panel (A) shows the distribution of the charge density ρ_{ch} calculated using the Skyrme parameterization Sk35-Skzs* investigated in the present study, along with the experimental charge distributions for the nucleus ^{70}Ge. The results calculations with the Skyrme parameterization of the ρ_{ch} shows agreement to the experimental data[83]. Figure (3.3) panel (B) shows the C0 charge form factor for the state $(J^\pi T = 0_1^+1)$ of ^{70}Ge nucleus calculated using Tassie and Bohr-Mottelson models, respectively. The effective interaction jun45 is used to

generate the wave functions used to calculate the one body transition densities (OBTD) and the overlapping to calculate the form factors using the model space only.

The theoretical results for the Tassie and Bohr-Mottelson models describe the experimental data very well through all regions at momentum transfer q and the results on Bohr-Mottelson are more able to reproduce the C0 form factors in all diffraction maxima regions.

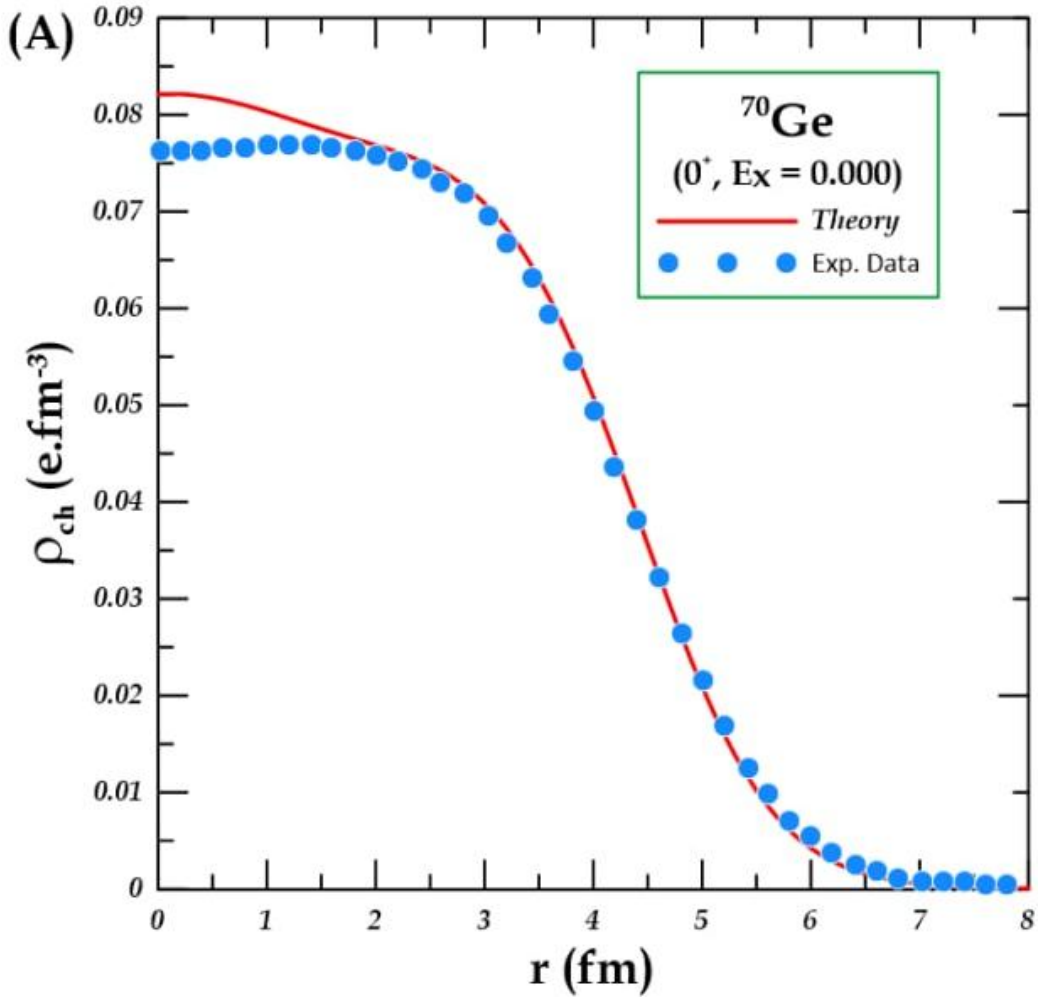

Figure (3.3): (A) The distribution of the charge density for the ^{70}Ge nucleus by utilizing Skyrme parameterization "Sk35-Skzs*", [83]

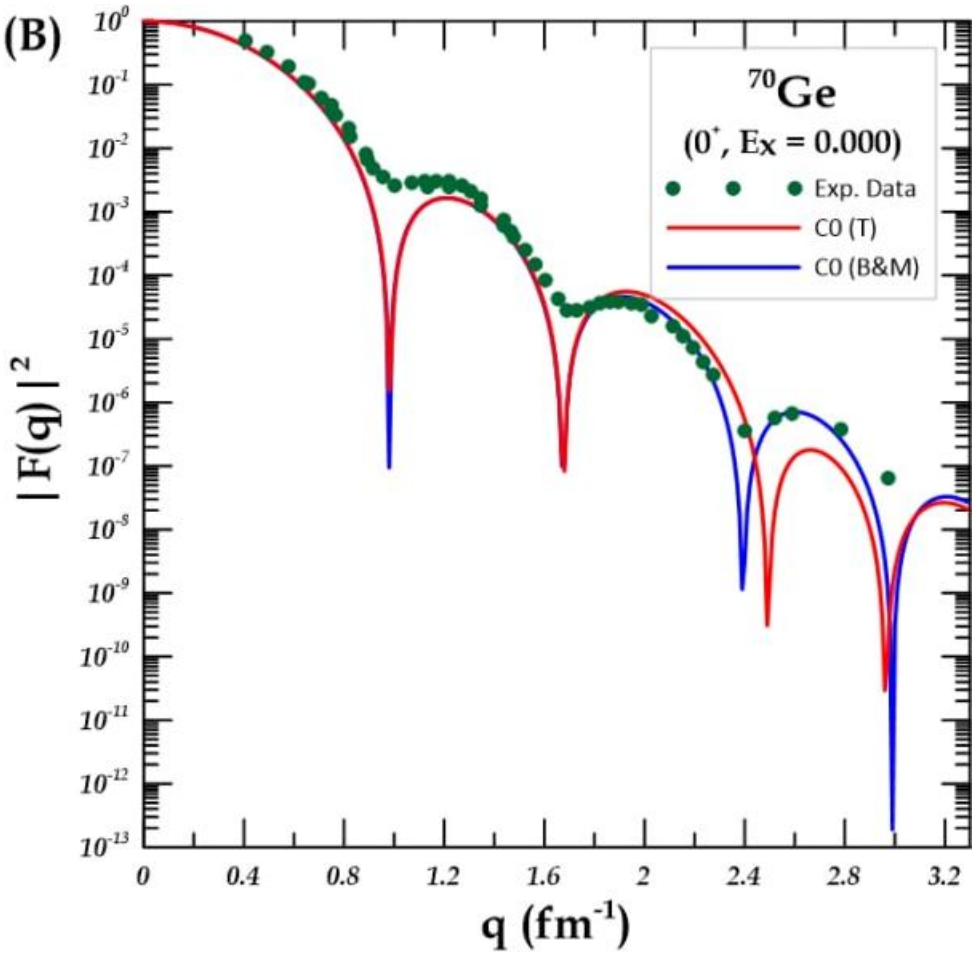

Figure (3.3): (B) C0 charge form factor for the 0_1^+1 state in ^{70}Ge nucleus, [83].

3.2.4 ^{72}Ge nucleus

The distribution of the charge density obtained for the ground state of the ^{72}Ge nucleus have been carried out using Skyrme parameterization Sk35-Skzs* displays in Figure (3.3) panel (A) using the model space only. Theoretical results of the ρ_{ch} predict the experimental data very well after r > 2.0 fm. The C0 charge form factor for the state $(J^\pi T = 0_1^+1)$ of ^{72}Ge nucleus were calculated by Bohr-Mottelson and Tassie models. As illustrated in the Figure (3.3) panel (B), the calculations using the conventional shell model use a core of ^{56}Ni with four proton and twelve neutron valence particles outside the core. The C0

form factor calculated the model space only utilizing jun45 effective interaction and Skyrme-parametrization (Sk35-Skzs*) agrees reasonably well with the measured data [87] .In all the momentum transfer regions and Bohr-Mottelson calculations reproduce the data very well better than Tassie calculations.

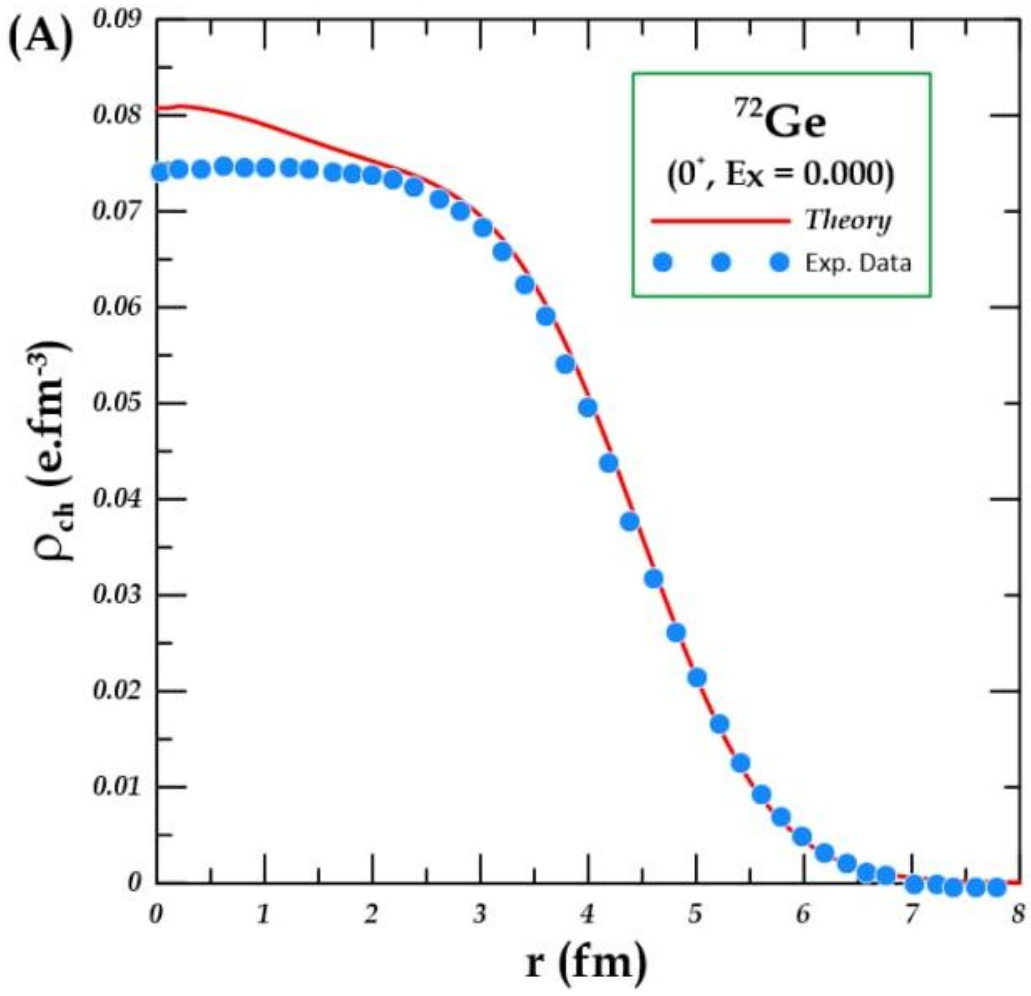

Figure (3.4): (A) The distribution of the charge density for the ^{72}Ge nucleus by utilizing Skyrme parameterization "Sk35-Skzs, [85].

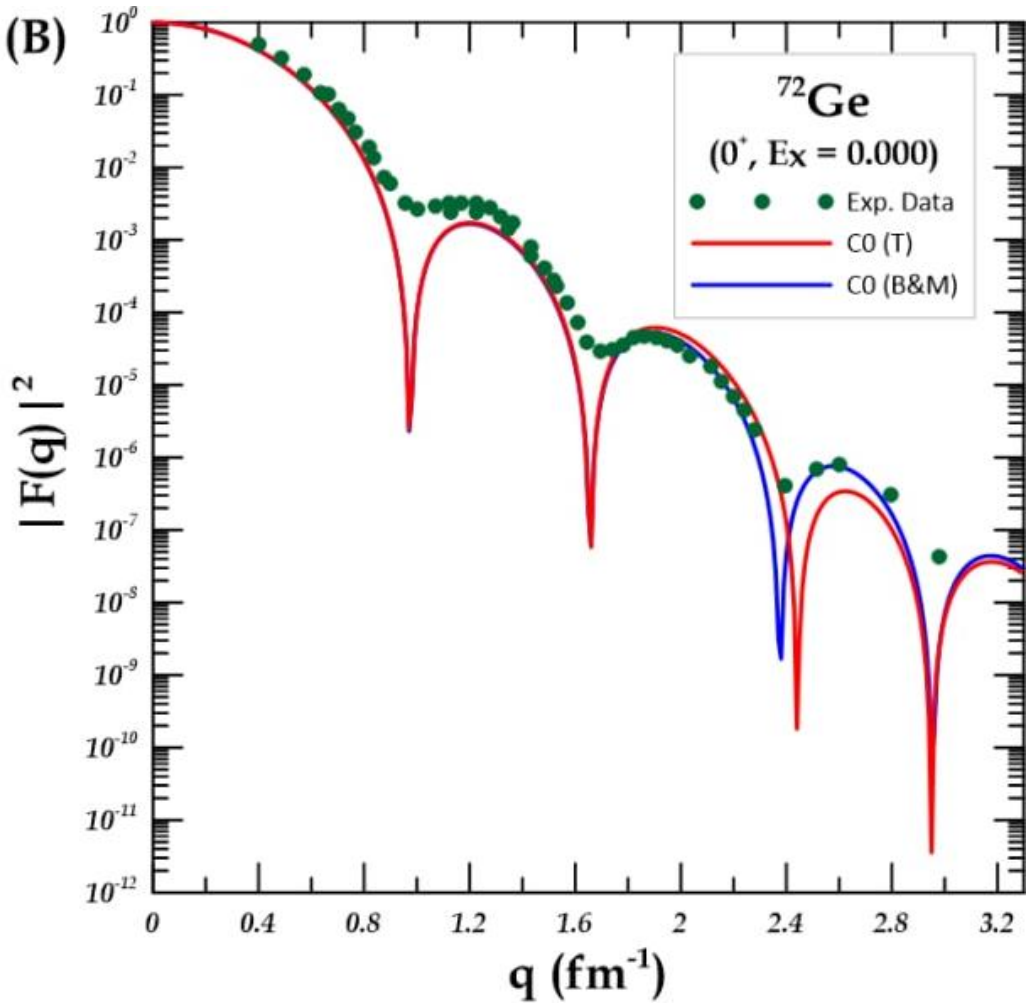

Figure (3.4): (B) C0 charge form factor for the 0_1^+1 state in ^{72}Ge nucleus, [85].

3.2.5 ^{74}Se nucleus

The theoretical results of the shell model calculation were carried out using the model space ($1f_{5/2}$, $2p_{3/2}$, $2p_{1/2}$, $1g_{9/2}$), which considers ^{56}Ni core with six protons and twelve neutrons outside the core for the ^{74}Se nucleus. Figure (3.2) panel (A) illustrates the ρ_{ch} calculated with the (Sk35-Skzs*) Skyrme parameterization used in this work, and the experimental charge distributions for the isotope ^{74}Se. The results calculations of the ρ_{ch} with the Skyrme parameterization shows equivalent to the experimental data [86].

The charge form factor C0 for the state $(J^{\pi}T = 0_1^{+}1)$ of ^{74}Se nucleus in fp-shell is presented in Figure (3.5) panel (B). The shell model computations employ the effective interaction (jun45), and the matrix element for interactions from beginning to final states is calculated using the residual interaction (Sk35-Skzs*). The measured data for C0 form is taken from [86]. The calculated form factor with the Tassie and Bohr-Mottelson models gives a very good agreement with the measured data spanned up to q=2.4 fm^{-1}

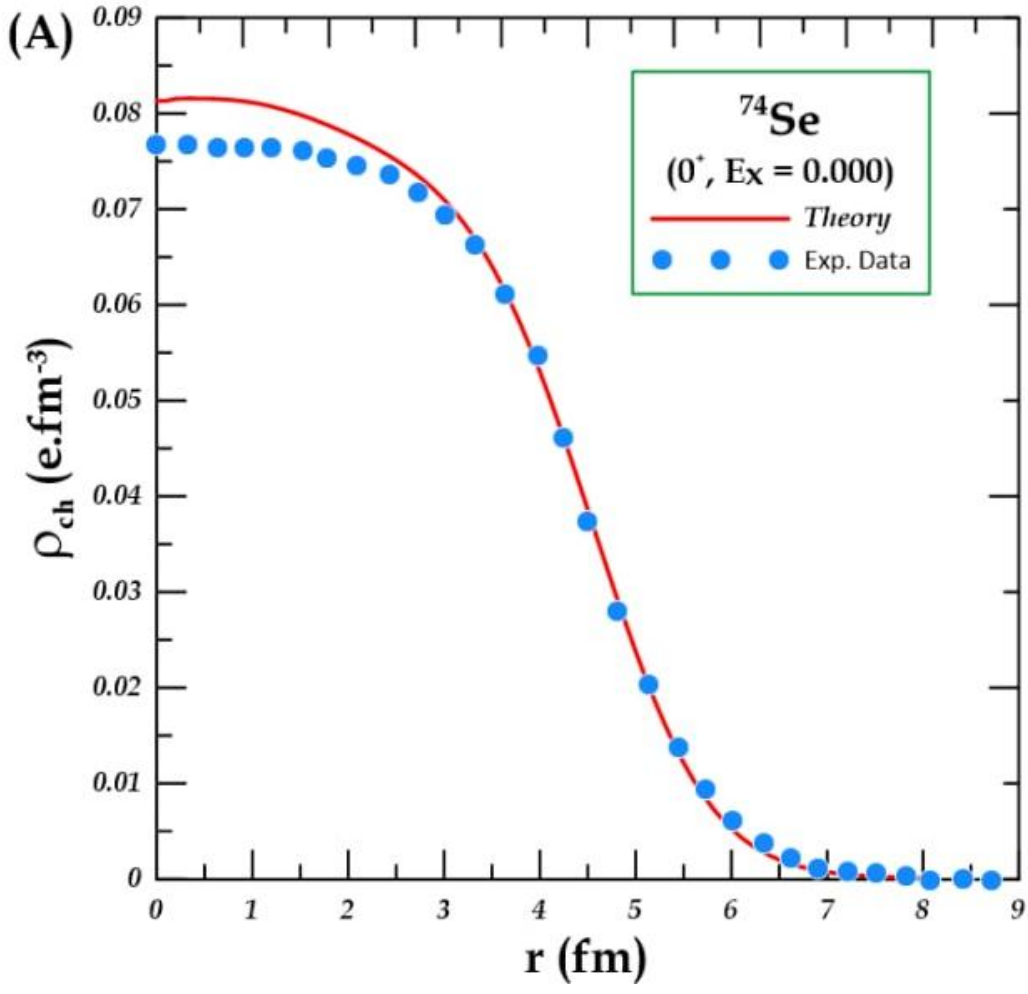

Figure (3.5): (A) The distribution of the charge density for the ^{74}Se nucleus by utilizing Skyrme parameterization "Sk35-Skzs*", [86].

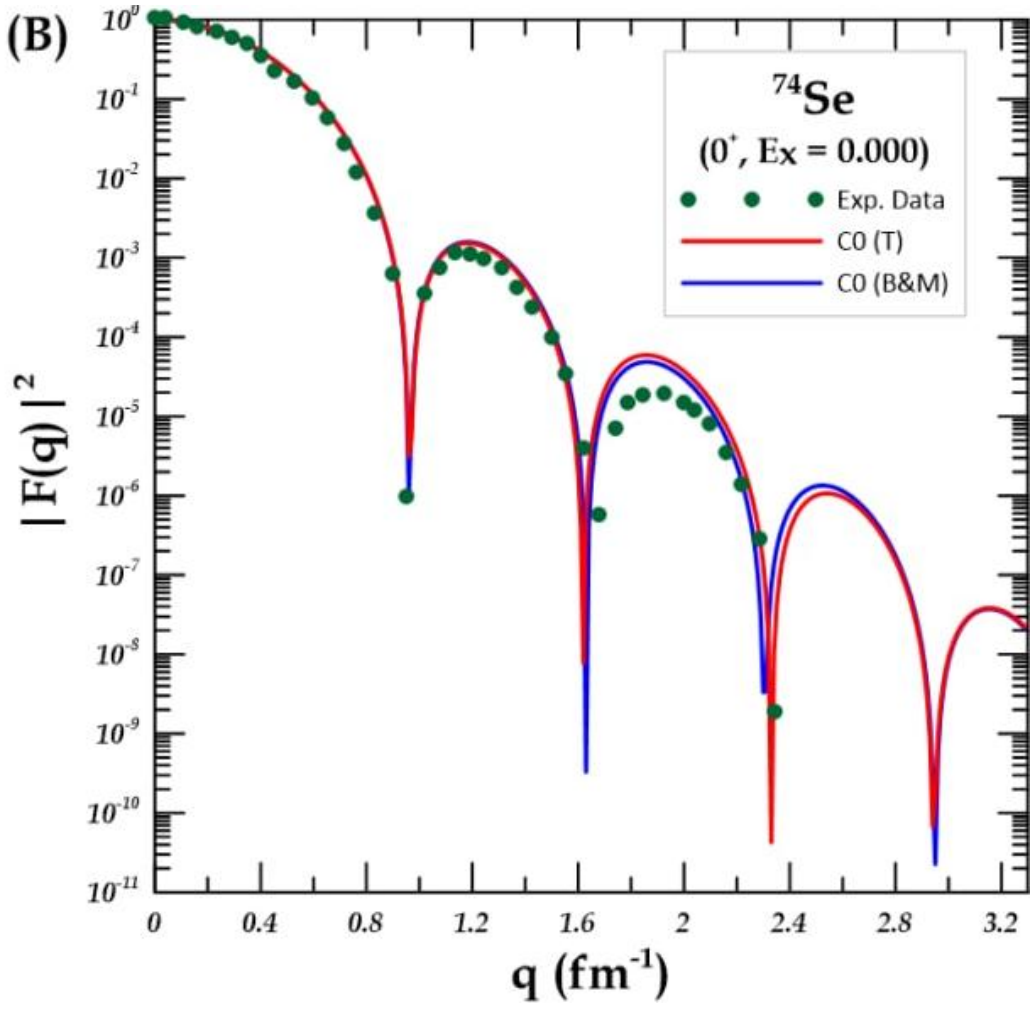

Figure (3.6): (B) C0 the charge form factor for the 0_1^+1 state in ^{74}Se nucleus, [86].

CHAPTER four : Conclusions and Suggestions for Future Works

Chapter Four

Conclusions and Suggestions for Future Works

4.1 Conclusions

The charge density distribution and charge form factors of elastic electron scattering for a few chosen fp-shell nuclei were studied in depth theoretically in the current work using Tassie and Bohr-Mottelson calculations. The theoretical calculation was carried out by employing the Skyrme parametrization with (Sk35-Skzs*).

After performing the present study, it can be concluded that:

1. The choice (Sk35-Skzs*) as residual effective interaction proves to be adequate for the calculation of the Tassie and Bohr-Mottelson models compared to the experimental data.
2. The model calculations for the ground state charge-density and C0 form factors are very successful in describing the experimental data without the need for effective charges to account for the core-polarization effect.
3. The calculated charge density distribution for the studied nuclei shows discripancy for low (r) values and agreed well as (r) increasing.
4. The calculated C0 form factors using Bohr and Mottelson collective model agreed reasonably well with the theoretical calculations and gave better results than Tassie Model calculations compared to the measured data for the studied nuclei.
5. The chosen effective interaction jun45 is adequate for the fpg model space which successful in reproducing the charge density distribution and the charge form factors for the ground state of the studied nuclei.

4.2 Suggestions for Future Works

It seems clear that further work is needed to find more identifiable features that could improve the calculations, and we therefore suggest the following

1. This work can be performed taking the core at ^{40}Ca which need considerable computer power and compare it with the present study might improve the calculations better.
2. Calculation other properties of the studied nuclei, the reduced electric quadruple probability B(E2) and the Electric ground state quadrupole moment Q.
3. Using the Skyrme-Hartree-Fock-Bogoliubov approach to perform the calculations and compare it with the present work**.**

Reference

References

[1] R.V.F Janssens, B Fornal, P.F Mantica, B.A Brown, R Broda, P Bhattacharyya, M.P Carpenter, M Cinausero, P.J Daly, A.D Davies, T Glasmacher, Z.W Grabowski, D.E Groh, M Honma, F.G Kondev, W Królas, T Lauritsen, S.N Liddick, S Lunardi, N Marginean, T Mizusaki, D.J Morrissey, A.C Morton, W.F Mueller, T Otsuka, T Pawlat, D Seweryniak, H Schatz, A Stolz, S.L Tabor, C.A Ur, G Viesti, I Wiedenhöver, J Wrzesiński,"Structure of $^{52, 54}$Ti and shell closures in neutron-rich nuclei above ^{48}Ca." *Phys. Lett. B*, vol. 546, no. 1–2, pp. 55–62, 2002.

[2] K. Kaneko, Y. Sun, T. Mizusaki, and M. Hasegawa, "Shell-model study for neutron-rich sd-shell nuclei," *Phys. Rev. C*, vol. 83, no. 1, pp.1-7 , 2011.

[3] O. Sorlin, "Gamma spectroscopy of nuclei far from stability," *Nucl. Phys. A*, vol. 685, pp. 186c-197c, 2000.

[4] M. Arnould, S. Goriely, and K. Takahashi, "The r-process of stellar nucleosynthesis: Astrophysics and nuclear physics achievements and mysteries," *Phys. Rep.*, vol. 450, no. 4–6, pp. 97–213, 2007.

[5] Y. K. Gambhir, S. Haq, and J. K. Suri, "Number conserving shell model for even Ca, Ti, Cr, and Fe isotopes," *Phys. Rev. C*, vol. 25, no. 1, pp. 630–649, 1982.

[6] K. Kaneko, Y. Sun, M. Hasegawa, and T. Mizusaki, "Shell model study of single-particle and collective structure in neutron-rich Cr isotopes," *Phys. Rev. C*, vol. 78, no. 6, pp.1-11: 064312,2008.

[7] B. A. Brown, "Towards the future of the nuclear shell model," *Nucl. Phys. A*, vol. 704, no. 1–4, pp. 11–20, 2002.

[8] M. G. Mayer, "On closed shells in nuclei. II," *Phys. Rev.*, vol. 75, no. 12, pp.1969–1970, 1949.

[9] J. H. D. Haxel, “Jensen, and HE Suess,” *Phys. Rev*, vol. 75, pp. 473–477, 1949.

[10] Otsuka, Takaharu, Takahiro Mizusaki, and Michio Honma. "Monte Carlo shell-model calculations." *Journal of Physics G: Nuclear and Particle Physics* 25.4: pp. 699-715 , 1999

[11] R. A. Radhi and A. Bouchebak, “Microscopic calculations of C2 and C4 form factors in sd-shell nuclei,” *Nucl. Phys. A*, vol. 716, pp. 87–99, 2003.

[12] K. Langanke, D. J. Dean, P. B. Radha, Y. Alhassid, and S. E. Koonin, “Shell-model Monte Carlo studies of fp-shell nuclei,” *Phys. Rev. C*, vol. 52, no. 2, pp.1–27, 1995.

[13] H. Überall and P. Uginčius, “Elastic and Inelastic Electron Scattering from Nuclear Multipole Moments in the First-Order Born Approximation,” *Phys. Rev.*, vol. 178, no. 4, pp.1–7, 1969.

[14] R. R. Roy and B. P. Nigam, *Nuclear physics: theory and experiment*,Wiley, 1967.

[15] J. M. Irvine, *Nuclear Structure Theory: International Series of Monographs in Natural Philosophy*, vol. 49. Elsevier, 2017.

[16] T. W. Donnelly and J. D. Walecka, “Elastic magnetic electron scattering and nuclear moments,” Nucl. Phys. A, vol. 201, no. 1, pp. 81–106, 1973.

[17] E. K. Warburton and D. J. Millener, “Structure of C 17 and N 17,” Phys. Rev. C, vol. 39, no. 3, pp. 1120-1129, 1989.

[18] H. Űberall, “Electron Scattering From Complex Nuclei. Part A.” Academic Press: New York and London, 1971.

[19] R. S. Willey, “Excitation of individual-particle states of nuclei by inelastic electron scattering,” *Nucl. Phys.*, vol. 40, pp. 529–565, 1963.

[20] N. F. Mott, "The scattering of fast electrons by atomic nuclei," *Proc. R. Soc. London. Ser. A, Contain. Pap. a Math. Phys. Character*, vol. 124, no. 794, pp. 425–442, 1929.

[21] R. Hofstadter, "Electron scattering and nuclear structure," Rev. Mod. Phys., vol. 28, no. 3, pp.214-253, 1956.

[22] A. Bohr and B.R. Mottelson, Nuclear structure. Vol. I. single-particle motion, New York, (1969).

[23] R. Machleidt, J. Negele and E. Vogt, Advances in Nuclear Physics, Vol.19 Plenum, New York, (1989).

[24] I. S. Gul'karov and L. D. Pinkus, "Charge density and octupole form factor of/sup 32/S," *Sov. J. Nucl. Phys.(Engl. Transl.);(United States)*, vol. 44, no. 2,pp. 210-213,1986.

[25] A. H. Wapstra, G. Audi, and R. Hoekstra, "Atomic masses from (mainly) experimental data," *At. Data Nucl. Data Tables*, vol. 39, no. 2, pp. 281–287, 1988.

[26] F. Petrovich, H. McManus, J. Borysowicz, and G. R. Hammerstein, "Core polarization in inelastic scattering," Phys. Rev. C, vol. 16, no. 2, pp. 839-872, 1977.

[27] L. J. Tassie, "A model of nuclear shape oscillations for g? Transitions and electron excitation," *Aust. J. Phys.*, vol. 9, no. 4, pp. 407–418, 1956.

[28] B. A. Brown, R. Radhi, and B. H. Wildenthal, "Electric quadrupole and hexadecupole nuclear excitations from the perspectives of electron scattering and modern shell-model theory," *Phys. Rep.*, vol. 101, no. 5, pp. 313–358, 1983.

[29] A. Bohr and B. R. Mottelson, "On the role of the δ resonance in the effective spin-dependent moments of nuclei," *Phys. Lett. B*, vol. 100, no. 1, pp. 10–12, 1981.

[30] S. S. Ghugre and S. N. Chintalapudi, "Effect of Configuration

Mixing and Core Excitation on Predominantly ($f_{7/2}$) n States in the Lower fp Shell Nuclei," *EPJ direct*, vol. 1, no. 1, pp. 1–10, 2000.

[31] R. A. Radhi, A. A. Abdullah, Z. A. Dakhil, and N. M. Adeeb, "Core-polarization effects on C2 form factors of p-shell nuclei," *Nucl. Phys. A*, vol. 696, no. 3–4, pp. 442–452, 2001.

[32] R. A. Radhi, "Nuclear structure study with inelastic electron scattering from 27Al," *Nucl. Phys. A*, vol. 707, no. 1–2, pp. 56–64, 2002.

[33] R. A. Radhi, "Single-particle quadrupole electromagnetic transitions in p-shell and sd-shell nuclei," *Eur. Phys. J. A-Hadrons Nucl.*, vol. 16, no. 3, pp. 387–392, 2003.

[34] N. A. Smirnova, A. De Maesschalck, A. Van Dyck, and K. Heyde, "Shell-model description of monopole shift in neutron-rich Cu," *Phys. Rev. C*, vol. 69, no. 4, pp. 1-11, 2004.

[35] B. V Danilin, S. N. Ershov, and J. S. Vaagen, "Charge and matter radii of Borromean halo nuclei: The He 6 nucleus," *Phys. Rev. C*, vol. 71, no. 5, pp. 1-5, 2005.

[36] F. Ying and Z.-Z. REN, "Theoretical studies on electron scattering of S and Si isotopes," *Chinese Phys. C*, vol. 30, no. 10, pp. 983–987, 2006.

[37] R. A. Radhi, "Perturbative role in the inelastic electron scattering from ^{29}Si," *Eur. Phys. J. A*, vol. 34, no. 1, pp. 107–111, 2007.

[38] X. Roca-Maza, M. Centelles, F. Salvat, and X. Vinas, "Theoretical study of elastic electron scattering off stable and exotic nuclei," *Phys. Rev. C*, vol. 78, no. 4, pp.1-18, 2008.

[39] O. Moreno, P. Sarriguren, E. M. de Guerra, J. M. Udias, T. W. Donnelly, and I. Sick, "Nuclear isospin mixing and elastic parity-violating electron scattering," *Nucl. Phys. A*, vol. 828, no. 3–4, pp. 306–332, 2009.

[40] S. Goriely, N. Chamel, and J. M. Pearson, "Further explorations of Skyrme-Hartree-Fock-Bogoliubov mass formulas. XII. Stiffness and stability of neutron-star matter," *Phys. Rev. C*, vol. 82, no. 3, pp. 1-48, 2010.

[41] A. K. Hamoudi, "Calculation of the longitudinal electron scattering form factors for the 2s-1d shell nuclei," *Iraqi J. Phys.*, vol. 9, no. 14, pp. 47–56, 2011.

[42] A. K. Hamoudi, M. A. Hasan, and A. R. Ridha, "Nucleon momentum distributions and elastic electron scattering form factors for some 1p-shell nuclei," *Pramana*, vol. 78, no. 5, pp. 737–748, 2012.

[43] R. A. Radhi, A. K. Hamoudi, and A. R. Ridha, "Elastic Electron Scattering From Unstable Neutron-Rich P," *Iraqi J. Sci.*, vol. 54, no. 2.2013, pp. 324–332, 2013.

[44] L. N.-R. Exotic, "Department of Physics and Astronomy and National Superconducting Cyclotron Laboratory, Michigan State University, East Lansing, MI 48824, USA, vol. 1, pp.1-20, 2001

[45] A. A. Al-Sammarraie, F. I. Sharrad, N. Yusof, and H. A. Kassim, "Longitudinal and transverse electron-nucleus scattering form factors of Mg 25," *Phys. Rev. C*, vol. 92, no. 3, pp.1-14, 2015.

[46] F. Z. Majeed, "Inelastic transverse magnetic dipole electron scattering form factors in 48Ca (restricted optimum configurations)," *Iraqi J. Phys.*, vol. 14, no. 30, pp. 9–17, 2016.

[47] A. N. Abdullah, "Matter density distributions and elastic form factors of some two-neutron halo nuclei," *Pramana*, vol. 89, no. 3, pp. 1–6, 2017.

[48] R. A. Radhi, A. A. Alzubadi, and A. H. Ali, "Magnetic dipole moments, electric quadrupole moments, and electron scattering form factors of neutron-rich s d− p f cross-shell nuclei," *Phys. Rev.*

C, vol. 97, no. 6, pp. 1-13, 2018.

[49] A. D. Salman, S. A. Al-Ramahi, and M. H. Oleiwi, "Inelastic electron-nucleus scattering form factors for 64, 66, 68Zn isotopes," in *AIP Conference Proceedings*, vol. 2144, no. 1, pp.1-16, 2019.

[50] A. A. Al-Rahmani and S. F. Kazem, "Elastic Electron-Nucleus Scattering Form Factors of Selected Medium Mass Nuclei," *NeuroQuantology*, vol. 18, no. 8, pp. 49-58, 2020.

[51] C. Chen, C. S. Fischer, C. D. Roberts, and J. Segovia, "Form factors of the nucleon axial current," *Phys. Lett. B*, vol. 815, pp. 1-6, 2021.

[52] M. Kortelainen, Z. Sun, G. Hagen, W. Nazarewicz, T. Papenbrock, and P.-G. Reinhard, "Universal trend of charge radii of even-even Ca–Zn nuclei," *Phys. Rev. C*, vol. 105, no. 2, pp.1-7, 2022.

[53] P. E. Hodgson, "Practical applications of the shell model," *Nature*, vol. 272, no. 5655, p. 741-742, 1978.

[54] P. A. M. Dirac, "Generalized hamiltonian dynamics," *Can. J. Math.*, vol. 2, pp. 129–148, 1950.

[55] V. M. Villalba and A. Rincón Maggiolo, "Energy spectrum of a 2D Dirac electron in the presence of a constant magnetic field," *Eur. Phys. J. B-Condensed Matter Complex Syst.*, vol. 22, no. 1, pp. 31–35, 2001.

[56] I. N. Levine, Á. G. Ureña, and A. R. Gayo, *Fisicoquímica*, vol. 1. McGraw-Hill Madrid, 2004.

[57] J. Tennyson, "Electron–molecule collision calculations using the R-matrix method," *Phys. Rep.*, vol. 491, no. 2–3, pp. 29–76, 2010.

[58] N. Hoteling, "Structure of iron isotopes at the limits of the pf shell." University of Maryland, College Park, 2008.

[59] B.-A. Li, L.-W. Chen, and C. M. Ko, "Recent progress and new challenges in isospin physics with heavy-ion reactions," *Phys. Rep.*,

vol. 464, no. 4–6, pp. 113–281, 2008.

[60] W. A. Goddard III, "Improved quantum theory of many-electron systems. II. The basic method," *Phys. Rev.*, vol. 157, no. 1, p. 81-93, 1967.

[61] B. Nilsson-Almqvist and E. Stenlund, "Interactions between hadrons and nuclei: The Lund Monte Carlo-FRITIOF version 1.6," *Comput. Phys. Commun.*, vol. 43, no. 3, pp. 387–397, 1987.

[62] G. K. Nie, "Masses and radii of the nuclei with N≥ Z in an alpha-cluster model," *Int. J. Mod. Phys. E*, vol. 19, no. 05n06, pp. 1205–1211, 2010.

[63] E. Domany, S. Alexander, D. Bensimon, and L. P. Kadanoff, "Solutions to the Schrödinger equation on some fractal lattices," *Phys. Rev. B*, vol. 28, no. 6, p. 3110-3114, 1983.

[64] J.-M. Lihm and C.-H. Park, "Wannier Function Perturbation Theory: Localized Representation and Interpolation of Wave Function Perturbation," *Phys. Rev. X*, vol. 11, no. 4, pp. 1-25, 2021.

[65] R. H. Stuewer, "The origin of the liquid-drop model and the interpretation of nuclear fission," *Perspect. Sci.*, vol. 2, no. 1, pp. 76–129, 1994.

[66] U. D. Jentschura and V. G. Serbo, "Nuclear form factor, validity of the equivalent photon approximation and Coulomb corrections to muon pair production in photon–nucleus and nucleus–nucleus collisions," *Eur. Phys. J. C*, vol. 64, no. 2, pp. 309–317, 2009.

[67] T. de Forest Jr and J. D. Walecka, "Electron scattering and nuclear structure," *Adv. Phys.*, vol. 15, no. 57, pp. 1–109, 1966.

[68] K. Matsuyanagi, M. Matsuo, T. Nakatsukasa, K. Yoshida, N. Hinohara, and K. Sato, "Microscopic derivation of the Bohr–Mottelson collective Hamiltonian and its application to quadrupole shape dynamics," *Phys. Scr.*, vol. 91, no. 6, pp.9-13, 2016.

[69] D. L. Hill and J. A. Wheeler, "Nuclear constitution and the interpretation of fission phenomena," *Phys. Rev.*, vol. 89, no. 5, p. 1102-1145, 1953.

[70] X. N. Wang, "A pQCD-based approach to parton production and equilibration in high-energy nuclear collisions," *Phys. Rep.*, vol. 280, no. 5–6, pp. 287–371, 1997.

[71] A. N. Bohr and B. R. Mottelson, *Nuclear Structure (in 2 volumes)*. World Scientific Publishing Company, 1998.

[72] A. Bohr, "Rotational motion in nuclei," *Rev. Mod. Phys.*, vol. 48, no. 3, pp. 365-372, 1976.

[73] B. Mottelson, "Nobel Prize lecture," *Rev. Mod. Phys*, vol. 48, pp. 375-383, 1976.

[74] K. Sato and N. Hinohara, "Shape mixing dynamics in the low-lying states of proton-rich Kr isotopes," *Nucl. Phys. A*, vol. 849, no. 1, pp. 53–71, 2011.

[75] R. Jackiw, "Delta-function potentials in two-and three-dimensional quantum mechanics," *MAB Bég Meml.*, pp.1-8, 1991.

[76] M. Ghafouri, H. Sadeghi, and M. Torkiha, "Self-consistent description of the SHFB equations for 112Sn," *Results Phys.*, vol. 8, pp. 734–743, 2018.

[77] P. Sarriguren, O. Moreno, E. M. de Guerra, D. N. Kadrev, A. N. Antonov, and M. K. Gaidarov, "Elastic Magnetic Electron Scattering from odd-A Nuclei," in *Journal of Physics: Conference Series*, vol. 1555, no. 1, pp.1-8, 2020

[78] A. T. Kruppa, M. Bender, W. Nazarewicz, P.-G. Reinhard, T. Vertse, and S. Ćwiok, "Shell corrections of superheavy nuclei in self-consistent calculations," *Phys. Rev. C*, vol. 61, no. 3, pp. 1-12, 2000.

[79] A. J. Buchmann, E. Hernández, and A. Faessler, "Electromagnetic

properties of the Δ(1232)," *Phys. Rev. C*, vol. 55, no. 1, pp. 448–463, 1997.

[80] W. M. C. Foulkes, L. Mitas, R. J. Needs, and G. Rajagopal, "Quantum Monte Carlo simulations of solids," *Rev. Mod. Phys.*, vol. 73, no. 1, pp. 33-34, 2001.

[81] J. Friedrich and P.-G. Reinhard, "Skyrme-force parametrization: Least-squares fit to nuclear ground-state properties," *Phys. Rev. C*, vol. 33, no. 1, pp. 335-351, 1986.

[82] W. R. Webber, J. C. Kish, J. M. Rockstroh, Y. Cassagnou, R. Legrain, A. Soutoul, O. Testard, and C. Tull "Production cross sections of fragmentsfrombeams of 400E 650 mev per nucleon ^{9}Be, ^{11}B, ^{12}C, ^{14}N, ^{15}N, ^{16}O, ^{20}Ne, ^{22}Ne, ^{56}Fe, and ^{58}Ni nuclei in teracting in a liquid hydrogentarget. II. isotoic cross sections of fragments " *Astrophys. J.*, vol. 508, no. 2, pp. 949-958, 1998.

[83] H. De Vries, C. W. De Jager, and C. De Vries, "Nuclear charge-density-distribution parameters from elastic electron scattering," *At. Data Nucl. Data Tables*, vol. 36, no. 3, pp. 495–536, 1987.

[84] M. Aygun, O. Kocadag, and Y. Sahin, "Phenomenological and microscopic model analysis of elastic scattering reactions of ^{18}O by ^{24}Mg, ^{28}Si, ^{58}Ni, ^{64}Zn, ^{90}Zr, ^{120}Sn, and ^{208}Pb target nuclei," *Rev. Mex. física*, vol. 61, no. 6, pp. 414–420, 2015.

[85] A. Abdullah, "Charge density Distributions and Elastic Electron Scattering from ^{58}Ni, ^{64}Zn, ^{70}Ge and ^{76}Se nuclei using the occupation numbers of the states," *Diyala J. Pure Sci.*, vol. 13, no. 2, p.75-85, 2017.

[86] G. K. Mallot, "Electron Scattering of Germanium and Muonic atoms of Krypton as Contribution to the Systemic of the Nuclear Charge Densities ."

[87] A. A. Shabana, "Finite element incremental approach and exact

rigid body inertia," 1996.

[88] R. Sahu and S. P. Pandya, "Structure of nuclei in the regionA= 70," *Pramana*, vol. 32, no. 4, pp. 367–375, 1989.

Appendix

Appendix

NushellX@MSU Code

NuShellX@MSU is a series of wrapper programs designed by Alex Brown.Bill Rae NuShellX is a set of computer tools for calculating correct energies, eigenvectors, and spectroscopic overlaps for low-lying states in shell model Hamiltonian matrix calculations with extremely high basis dimensions. It uses a J-coupled proton-neutron basis with J-scheme matrices of up to 100 million dimensions. That creates NuShellX input from model space and Hamiltonian data files The wrapper scripts also convert NuShellX output into figures and tables for energy levels, gamma decay, and beta decay. The NuShellX code is built on a proton-neutron basis and uses a similar approach to NATHANA three-term sum may be used to express the Hamiltonian

$$H = \mathrm{H_{nn}} + \mathrm{H_{pp}} + \mathrm{H_{pn}}$$

The second quantized form for $\mathrm{H_{pn}}$ is

$$\mathrm{H_{pn}} = \sum_{\mathrm{pnp'n',J_0}} \left\{ \left[\mathrm{a_p^\dagger\ a_n^\dagger} \right]^{\mathrm{J_0}} \times \left[\mathrm{a_{p'}\ a_{n'}} \right]^{\mathrm{J_0}} \right\}^{(0)}$$

The NuShellX@MSU setup is shown in Figure In the center is NuShellX. Wrapper programs encircle it, pulling data from a database of previously created Hamiltonians (bottom left).

The Hamiltonians might also have obtained using ab-initio approaches like those outlined in references (top left) Finally, the wrapper combines theoretical energies with data from the Evaluated Nuclear Structure Data Files (ENSDF) to generate a graph that may be used to compare theory and experiment. For the operators a+, a+ a+, and a+ a, NuShellX takes the overlaps. The wrapper converts them into

spectroscopic factors, two-nucleon transfer amplitudes, and one-body transition densities. The one-body transition densities are used in combination with the program DENS to generate the matrix elements for the Ml, El, and Gamow-Teller (GT) operators

To construct a gamma-ray decay scheme, the magnetic and quadrupole moments for all states in the calculation are coupled with the M1 and E2 data. The GT matrix elements are used to obtain an acceptable beta-decay scheme.

The DENS program allows you to use radial wave functions from the harmonic-oscillator, Woods-Saxon, or Skyrme energy-density functions techniques for matrix elements. DENS may also be used to compute electron scattering form factors

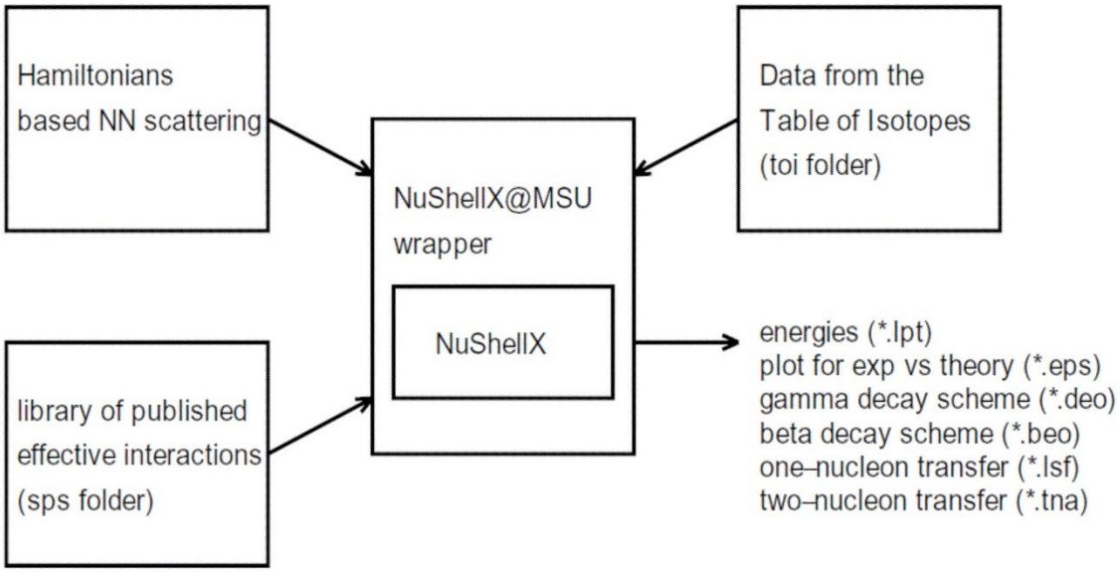

Schematic layout of the NuShellX@MSU codes.